Assessment of Ring Current Models for Monocycles

ELECTRONIC SUPPORTING INFORMATION

Guglielmo Monaco* and Riccardo Zanasi

Dipartimento di Chimica e Biologia

Università degli Studi di Salerno,

via Giovanni Paolo II, 84084 Fisciano (SA), Italy

E-mail: gmonaco@unisa.it

*To whom correspondence should be addressed

Table 1: Values of average ring radii (Å) estimated from the contribution of π orbitals to the parallel component of the magnetic shielding ($\sigma_{\parallel,\pi}$) according to different RCMs, and the geometrical value $P/(2\pi)$, which for regular polygons is intermediate between the inradius and the circumradius. The mean absolute percentage deviation (MAPD) of the model radii from the geometrical value is reported on the last line.

Species	ICLOC	ICLOC2	TCLOC	ETCLOC	TCLOC2	$\frac{P}{2\pi}$
$C_3H_3^+$	1.302	0.879	0.823	1.046	0.722	0.651
C_3H_6	1.429	1.320	1.429	1.247	1.265	0.714
$C_4H_4^{2+}$	1.665	1.019	0.932	1.178	1.019	0.921
$C_4H_4^{2-}$	1.832	1.343	1.146	1.359	1.127	0.916
C_4H_4	1.577	0.890	0.839	1.068	0.890	0.916
$C_5H_5^-$	1.930	1.449	1.237	1.533	1.170	1.116
C_6H_6	1.995	1.536	1.313	1.616	1.224	1.332
$C_6H_3^+$	1.907	1.481	1.270	1.558	1.478	1.475
C_6I_6	1.975	1.551	1.321	1.621	1.241	1.338
$C_6I_6^{2+}$	1.972	1.560	1.326	1.108	1.255	1.331
$C_7H_7^+$	2.115	1.683	1.434	1.754	1.683	1.555
$C_8H_8^{2+}$	2.243	1.834	1.560	1.896	1.477	1.761
$C_8H_8^{2-}$	2.440	2.077	1.766	2.123	1.712	1.804
C_8H_8	2.113	1.674	1.429	1.748	1.674	1.782
$C_9H_9^-$	2.525	2.180	1.858	2.222	1.808	1.991
$C_{10}H_{10}$	2.669	2.344	2.005	2.381	1.958	2.207
furan	1.795	1.412	1.204	1.477	1.412	1.080
pyrrole	1.817	1.379	1.179	1.457	1.100	1.091
thiophene	2.035	1.490	1.286	1.595	1.186	1.201
N_4^{2-}	1.605	1.172	1.002	1.206	0.955	0.856
N_6	1.704	1.317	1.126	1.386	1.317	1.222
O_3	1.299	1.368	1.299	0.870	0.885	0.649
O_4^{2+}	1.352	1.019	0.877	1.083	1.019	0.807
borazine	2.718	2.384	2.226	1.316	1.391	1.359
boroxine	2.600	1.569	2.243	1.242	1.269	1.300
Al_3^-	2.476	1.716	1.661	2.111	1.484	1.238
Al_4^{2-}	3.268	1.912	1.849	2.335	1.618	1.634
Si_6H_6	3.120	2.249	1.960	2.416	1.823	2.110
P_6	2.788	2.070	1.791	2.204	1.660	1.990
S_6	1.625	1.108	1.011	1.256	0.738	2.001
Ga_3^-	2.500	1.739	1.711	2.174	1.505	1.250
Ga_4^{2-}	3.306	2.149	2.040	1.707	1.902	1.653
MAPD	64.7	26.5	22.4	27.4	14.9	

Table 2: Values of average ring radii (Å) estimated from the contribution of σ orbitals to the parallel component of the magnetic shielding ($\sigma_{\parallel,\sigma}$) according to different RCMs, and the geometrical value $P/(2\pi)$, which for regular polygons is intermediate between the inradius and the circumradius. The mean absolute percentage deviation (MAPD) of the model radii from the geometrical value is reported on the last line.

Species	ICLOC	ICLOC2	TCLOC	ETCLOC	TCLOC2	$\frac{P}{2\pi}$
H_6	1.220	1.216	1.220	0.933	1.213	0.939
$C_3H_3^+$	1.302	1.270	1.101	1.101	1.102	0.651
C_3H_6	1.429	1.329	1.116	1.116	1.116	0.714
$C_4H_4^{2+}$	0.484	0.344	0.311	0.385	0.224	0.921
$C_4H_4^{2-}$	0.483	0.342	0.310	0.384	0.222	0.916
C_4H_4	0.613	0.462	0.410	0.501	0.315	0.916
$C_5H_5^-$	0.334	0.227	1.286	1.286	1.286	1.116
C_6H_6	0.458	0.314	0.287	1.990	0.197	1.332
$C_6H_3^+$	1.640	1.640	1.640	1.365	1.640	1.475
C_6I_6	0.684	0.499	0.447	0.551	0.326	1.338
$C_6I_6^{2+}$	2.662	2.298	2.174	2.174	2.174	1.331
$C_7H_7^+$	0.529	0.364	0.529	2.229	0.220	1.555
$C_8H_8^{2+}$	0.539	0.370	0.540	2.303	0.225	1.761
$C_8H_8^{2-}$	0.486	0.333	0.485	1.962	0.195	1.804
C_8H_8	0.808	0.575	0.808	2.806	0.367	1.782
$C_9H_9^-$	0.542	0.371	0.339	2.112	0.226	1.991
$C_{10}H_{10}$	0.544	0.372	2.204	2.204	2.204	2.207
furan	0.312	0.212	1.193	1.193	1.193	1.080
pyrrole	0.324	0.221	1.231	1.231	1.231	1.091
thiophene	2.402	0.806	1.313	1.313	1.313	1.201
N_4^{2-}	0.575	0.467	0.575	0.489	0.353	0.856
N_6	0.515	0.365	0.330	1.802	0.232	1.222
O_3	0.975	0.975	0.975	1.007	0.975	0.649
O_4^{2+}	0.519	0.429	0.372	0.446	0.332	0.807
borazine	0.520	0.360	0.521	2.175	0.219	1.359
boroxine	0.496	0.344	0.314	2.022	0.214	1.300
Al_3^-	2.374	2.374	2.374	2.456	2.374	1.238
Al_4^{2-}	2.470	2.470	2.470	2.536	2.470	1.634
Si_6H_6	0.631	0.432	0.631	2.673	0.267	2.110
P_6	0.511	0.349	1.903	1.903	1.903	1.990
S_6	4.002	1.410	1.898	1.898	1.898	2.001
Ga_3^-	2.500	2.442	2.053	2.053	2.053	1.250
Ga_4^{2-}	2.469	2.469	2.469	2.498	2.469	1.653
MAPD	64.9	66.3	49.7	38.5	56.2	

Table 3: Best fit values of the displacements from the molecular plane and the standard deviations of the loops according to various RCMs applied to the π contribution to $\sigma_{\parallel}$ scans. All entries in Å.

	$\langle z \rangle$		ρ			ζ
Species	ICLOC2	TCLOC2	TCLOC	ETCLOC	TCLOC2	ETCLOC
$C_3H_3^+$	0.640	0.190	0.873	0.006	0.842	0.556
C_3H_6	2.193	0.679	2.063	2.946	2.380	2.546
$C_4H_4^{2+}$	0.680	0.680	0.952	0.007	0.004	0.590
$C_4H_4^{2-}$	0.705	0.113	1.080	0.650	1.075	0.830
C_4H_4	0.662	0.662	0.897	0.001	0.002	0.575
$C_5H_5^-$	0.681	0.222	1.097	0.022	1.084	0.606
C_6H_6	0.684	0.268	1.130	0.055	1.113	0.611
$C_6H_3^+$	0.650	0.650	1.080	0.040	0.100	0.578
C_6I_6	0.658	0.259	1.115	0.066	1.099	0.592
$C_6I_6^{2+}$	0.650	0.246	1.112	1.275	1.098	1.205
$C_7H_7^+$	0.692	0.692	1.190	0.000	0.012	0.620
$C_8H_8^{2+}$	0.699	0.307	1.251	0.000	1.232	0.630
$C_8H_8^{2-}$	0.694	0.287	1.338	0.001	1.320	0.635
C_8H_8	0.696	0.696	1.190	0.012	0.019	0.622
$C_9H_9^-$	0.691	0.295	1.372	0.003	1.352	0.635
$C_{10}H_{10}$	0.691	0.317	1.430	0.020	1.405	0.639
furan	0.601	0.601	1.015	0.043	0.019	0.537
pyrrole	0.636	0.236	1.032	0.000	1.017	0.564
thiophene	0.737	0.268	1.159	0.000	1.139	0.650
N_4^{2-}	0.582	0.164	0.914	0.445	0.904	0.640
N_6	0.585	0.585	0.967	0.021	0.011	0.520
O_3	1.242	0.478	1.482	1.734	1.375	1.515
O_4^{2+}	0.479	0.479	0.770	0.014	0.015	0.423
borazine	1.036	0.714	1.695	2.068	1.607	1.850
boroxine	1.947	0.652	2.708	2.624	2.120	2.293
Al_3^-	1.353	0.352	1.830	0.036	1.764	1.190
Al_4^{2-}	1.448	0.419	1.985	0.000	1.903	1.267
Si_6H_6	1.103	0.379	1.751	0.066	1.721	0.975
P_6	0.974	0.362	1.571	0.003	1.545	0.861
S_6	0.666	0.700	0.952	0.002	0.623	0.563
Ga_3^-	1.412	0.378	1.903	0.025	1.823	1.244
Ga_4^{2-}	1.569	0.348	2.179	2.341	2.130	2.208

Table 4: Best fit values of the displacements from the molecular plane and the standard deviations of the loops according to various RCMs applied to the σ contribution to $\sigma_{\parallel}$ scans. All entries in Å.

	$\langle z \rangle$		ρ			ζ
Species	ICLOC2	TCLOC2	TCLOC	ETCLOC	TCLOC2	ETCLOC
H_6	0.057	0.048	0.001	0.753	0.100	0.716
$C_3H_3^+$	0.790	0.000	1.130	1.130	1.131	1.130
C_3H_6	0.634	0.000	1.015	1.015	1.015	1.015
$C_4H_4^{2+}$	0.199	0.214	0.284	0.000	0.199	0.165
$C_4H_4^{2-}$	0.200	0.216	0.284	0.000	0.199	0.166
C_4H_4	0.228	0.245	0.352	0.000	0.262	0.193
$C_5H_5^-$	0.164	0.000	2.991	2.991	2.991	2.991
C_6H_6	0.212	0.231	0.278	6.000	0.189	0.014
$C_6H_3^+$	0.000	0.000	0.003	1.128	0.003	1.020
C_6I_6	0.272	0.294	0.399	0.000	0.286	0.228
$C_6I_6^{2+}$	1.947	0.000	2.578	2.578	2.578	2.578
$C_7H_7^+$	0.244	0.264	0.001	6.000	0.217	0.014
$C_8H_8^{2+}$	0.257	0.275	0.009	6.000	0.223	0.011
$C_8H_8^{2-}$	0.242	0.262	0.031	4.287	0.202	4.429
C_8H_8	0.337	0.363	0.001	4.697	0.333	0.000
$C_9H_9^-$	0.268	0.285	0.336	4.830	0.226	4.970
$C_{10}H_{10}$	0.277	0.000	4.869	4.868	4.867	4.868
furan	0.153	0.000	2.794	2.794	2.794	2.794
pyrrole	0.158	0.000	2.911	2.911	2.911	2.911
thiophene	1.677	0.000	2.435	2.435	2.435	2.435
N_4^{2-}	0.186	0.191	0.009	0.000	0.259	0.163
N_6	0.214	0.233	0.303	3.089	0.212	0.000
O_3	0.000	0.000	0.001	0.178	0.001	0.029
O_4^{2+}	0.161	0.162	0.287	0.001	0.237	0.142
borazine	0.233	0.254	0.003	6.000	0.213	0.058
boroxine	0.218	0.238	0.296	5.164	0.203	0.000
Al_3^-	0.000	0.000	0.001	0.504	0.001	0.220
Al_4^{2-}	0.000	0.000	0.001	0.391	0.000	0.000
Si_6H_6	0.307	0.329	0.001	4.694	0.263	6.000
P_6	0.253	0.000	4.602	4.602	4.602	4.602
S_6	2.150	0.000	2.877	2.877	2.877	2.877
Ga_3^-	0.603	0.000	1.416	1.416	1.416	1.416
Ga_4^{2-}	0.000	0.000	0.001	0.257	0.000	0.018

Table 5: Best fit parameters of the ICLOC2C model. Signed current strengths are in nA T^{-1}, loop radii in Å.

	π electrons				σ electrons			
Species	$\overline{I_1^{\mathrm{B}}}$	s_1	$\overline{I_2^{\mathrm{B}}}$	s_2	$\overline{I_1^{\mathrm{B}}}$	s_1	$\overline{I_2^{\mathrm{B}}}$	s_2
H_6	–	–	–	–	-13.54	1.22	0.31	1.39
$C_3H_3^+$	-7.75	1.00	3.53	0.64	-10.73	1.30	4.26	0.78
C_3H_6	-1.45	1.43	1.08	1.08	-13.26	1.38	3.66	0.79
$C_4H_4^{2+}$	-7.06	1.15	2.76	0.70	10.11	0.80	-8.43	1.66
$C_4H_4^{2-}$	-14.27	1.45	3.79	0.78	9.26	0.82	-8.01	1.72
C_4H_4	24.30	1.11	-7.30	0.55	11.26	0.85	-6.70	1.83
$C_5H_5^-$	-16.50	1.52	4.53	0.90	-8.76	1.92	6.55	0.88
C_6H_6	-17.12	1.58	4.82	0.97	-7.43	2.22	6.35	0.99
$C_6H_3^+$	-9.73	1.52	2.75	0.95	-8.36	1.89	-1.02	0.73
C_6I_6	-14.19	1.59	3.67	0.96	4.73	1.07	-3.73	2.68
$C_6I_6^{2+}$	-14.15	1.60	3.64	0.97	-31.11	2.66	15.19	1.58
$C_7H_7^+$	-16.28	1.73	3.81	1.03	6.31	1.13	-7.14	2.45
$C_8H_8^{2+}$	-16.53	1.86	3.92	1.15	-6.31	2.82	5.11	1.21
$C_8H_8^{2-}$	-24.10	2.12	4.09	1.22	-5.95	2.73	4.52	1.31
C_8H_8	23.76	1.76	-4.74	0.97	5.56	1.31	-4.71	3.14
$C_9H_9^-$	-24.84	2.21	4.30	1.33	-5.12	3.13	3.83	1.36
$C_{10}H_{10}$	-24.03	2.38	3.33	1.37	-5.33	3.27	3.89	1.54
furan	-10.70	1.44	2.93	0.89	-8.32	1.81	6.16	0.81
pyrrole	-13.87	1.43	3.92	0.87	-8.49	1.88	6.31	0.83
thiophene	-13.27	1.56	4.10	0.95	-9.60	1.86	6.40	0.93
N_4^{2-}	-13.28	1.24	3.73	0.71	12.79	0.71	-5.52	1.26
N_6	-15.55	1.37	3.90	0.80	7.65	0.83	-6.42	1.95
O_3	-2.52	1.30	1.67	1.00	-11.66	0.98	0.27	0.98
O_4^{2+}	-9.79	1.05	3.07	0.67	10.85	0.60	-3.43	1.24
borazine	-3.45	2.49	1.47	1.95	-6.56	2.28	6.16	1.03
boroxine	-2.57	2.60	1.65	1.88	-6.91	1.96	6.82	0.99
Al_3^-	-9.06	2.01	4.52	1.31	-7.84	2.48	-0.50	1.42
Al_4^{2-}	-9.04	2.26	4.11	1.43	-24.60	2.47	0.85	2.46
Si_6H_6	-17.05	2.43	4.37	1.38	-5.42	3.38	4.27	1.52
P_6	-17.69	2.16	5.40	1.35	-7.85	2.93	5.87	1.29
S_6	3.61	2.72	-3.04	3.68	-9.47	2.69	5.04	1.29
Ga_3^-	-8.85	2.11	4.13	1.31	-7.12	2.50	0.33	0.89
Ga_4^{2-}	-7.89	2.59	3.05	1.48	-25.46	2.47	0.53	2.47

Table 6: Residual sum of squares (RSS) for the fits of the $\sigma_{\|,\pi}$ scans.

Species	ICLOC	ICLOC2	ICLOC2C	TCLOC	ETCLOC	TCLOC2
$C_3H_3^+$	1.16e+02	1.79e+00	7.14e+00	5.58e+00	1.44e+00	1.78e+00
C_3H_6	2.58e+01	3.77e+00	1.73e+01	1.30e+01	5.14e-02	3.85e-01
$C_4H_4^{2+}$	5.70e+01	6.70e-01	5.66e+00	4.16e+00	1.13e+00	6.70e-01
$C_4H_4^{2-}$	1.23e+02	9.90e+00	2.64e+00	9.52e-01	7.75e-01	8.19e-01
C_4H_4	1.44e+03	2.94e+01	1.75e+02	1.05e+02	3.05e+01	2.94e+01
$C_5H_5^-$	9.00e+01	2.33e+00	4.66e+00	2.13e+00	5.21e-02	4.30e-01
C_6H_6	7.29e+01	5.62e-01	5.46e+00	3.23e+00	3.87e-01	5.12e-01
$C_6H_3^+$	2.36e+01	4.29e-02	2.69e+00	1.85e+00	5.02e-01	4.29e-02
C_6I_6	4.38e+01	7.66e-01	2.97e+00	1.56e+00	3.01e-01	1.53e-01
$C_6I_6^{2+}$	4.07e+01	1.03e+00	2.38e+00	1.19e+00	2.43e-01	1.66e-01
$C_7H_7^+$	4.97e+01	2.18e-01	4.23e+00	2.26e+00	2.85e-01	2.18e-01
$C_8H_8^{2+}$	3.38e+01	1.41e-01	2.49e+00	1.33e+00	1.31e-01	9.97e-02
$C_8H_8^{2-}$	4.31e+01	4.08e-01	2.57e+00	8.92e-01	1.69e-02	1.02e-01
C_8H_8	1.21e+02	3.40e-01	1.28e+01	6.40e+00	1.06e+00	3.40e-01
$C_9H_9^-$	3.39e+01	2.85e-01	1.85e+00	6.26e-01	2.61e-03	2.82e-02
$C_{10}H_{10}$	2.31e+01	1.20e-01	1.47e+00	4.53e-01	6.24e-03	2.43e-02
furan	2.74e+01	9.31e-02	2.45e+00	1.52e+00	2.54e-01	9.31e-02
pyrrole	6.19e+01	7.20e-01	4.38e+00	2.52e+00	2.46e-01	4.77e-01
thiophene	6.07e+01	6.73e-01	4.41e+00	2.68e+00	3.23e-01	4.26e-01
N_4^{2-}	9.04e+01	3.94e+00	3.46e+00	1.37e+00	1.01e-01	3.21e-01
N_6	7.82e+01	2.85e-01	7.57e+00	4.35e+00	7.13e-01	2.85e-01
O_3	2.85e+01	4.69e+00	1.13e+01	8.09e+00	1.45e-01	2.37e-01
O_4^{2+}	4.33e+01	3.93e-02	4.91e+00	3.50e+00	9.27e-01	3.93e-02
borazine	4.58e+00	2.31e+00	2.77e+00	2.74e+00	9.41e-02	1.17e-01
boroxine	1.42e+01	2.48e+00	4.06e+00	3.98e+00	9.73e-02	9.10e-02
Al_3^-	1.03e+02	2.68e+00	2.36e+00	1.74e+00	2.42e-01	4.50e-01
Al_4^{2-}	5.20e+01	9.81e-01	3.44e+00	2.63e+00	7.96e-01	7.90e-01
Si_6H_6	5.90e+01	9.01e-01	3.59e+00	1.68e+00	1.26e-01	1.64e-01
P_6	5.62e+01	5.10e-01	3.59e+00	2.14e+00	2.58e-01	2.38e-01
S_6	2.79e+00	9.56e-01	2.49e-01	1.56e+00	1.28e+00	6.75e-01
Ga_3^-	1.24e+02	2.82e+00	3.14e+00	2.19e+00	3.63e-01	3.68e-01
Ga_4^{2-}	5.13e+01	2.76e+00	6.82e-01	2.51e-01	7.66e-03	1.31e-03

Table 7: Residual sum of squares (RSS) for the fits of the $\sigma_{\|,\sigma}$ scans.

Species	ICLOC	ICLOC2	ICLOC2C	TCLOC	ETCLOC	TCLOC2
H_6	2.25e-01	2.18e-01	2.20e-01	2.25e-01	1.10e-01	2.17e-01
$C_3H_3^+$	4.66e+02	1.71e+01	2.85e+00	3.25e-01	3.25e-01	3.25e-01
C_3H_6	2.93e+02	9.57e+00	1.13e-01	1.76e-01	1.76e-01	1.76e-01
$C_4H_4^{2+}$	6.01e+02	4.50e+02	4.01e+00	5.13e+02	4.84e+02	4.09e+02
$C_4H_4^{2-}$	5.49e+02	4.25e+02	1.80e+00	4.77e+02	4.53e+02	3.91e+02
C_4H_4	3.27e+02	1.91e+02	3.51e+00	2.40e+02	2.15e+02	1.59e+02
$C_5H_5^-$	1.02e+03	9.74e+02	1.25e+00	7.50e-01	7.50e-01	7.50e-01
C_6H_6	5.86e+02	5.31e+02	1.72e+00	5.57e+02	7.36e+01	5.15e+02
$C_6H_3^+$	1.45e+01	1.45e+01	2.86e-02	1.45e+01	6.05e-02	1.45e+01
C_6I_6	1.11e+02	8.51e+01	6.51e-01	9.57e+01	9.06e+01	7.81e+01
$C_6I_6^{2+}$	2.66e+03	2.54e+02	3.28e+01	4.23e+01	4.23e+01	4.23e+01
$C_7H_7^+$	4.29e+02	3.84e+02	1.10e+00	4.29e+02	4.86e+01	3.70e+02
$C_8H_8^{2+}$	3.77e+02	3.46e+02	1.38e+00	3.77e+02	7.08e+01	3.36e+02
$C_8H_8^{2-}$	2.86e+02	2.71e+02	3.73e-01	2.86e+02	9.63e-02	2.67e+02
C_8H_8	1.40e+02	1.07e+02	1.05e+00	1.40e+02	1.42e+01	9.72e+01
$C_9H_9^-$	2.26e+02	2.13e+02	5.65e-01	2.19e+02	4.90e-02	2.09e+02
$C_{10}H_{10}$	2.00e+02	1.91e+02	2.70e-01	1.67e-02	1.67e-02	1.67e-02
furan	1.07e+03	1.01e+03	1.90e+00	7.60e-01	7.60e-01	7.60e-01
pyrrole	1.08e+03	1.02e+03	1.96e+00	7.63e-01	7.63e-01	7.63e-01
thiophene	1.33e+03	6.32e+02	5.89e-01	6.70e-01	6.70e-01	6.70e-01
N_4^{2-}	1.20e+02	3.20e+01	5.06e+00	1.20e+02	4.21e+01	2.00e+01
N_6	4.49e+02	3.43e+02	5.90e+00	3.87e+02	7.72e+01	3.12e+02
O_3	2.83e+00	2.83e+00	2.83e+00	2.83e+00	1.89e-01	2.83e+00
O_4^{2+}	9.12e+01	1.72e+01	9.25e+00	3.49e+01	2.45e+01	8.87e+00
borazine	3.85e+02	3.35e+02	1.05e+00	3.85e+02	3.50e+01	3.20e+02
boroxine	3.59e+02	3.06e+02	5.73e-01	3.30e+02	3.85e+01	2.91e+02
Al_3^-	6.71e-01	6.71e-01	2.85e-01	6.71e-01	1.11e-01	6.71e-01
Al_4^{2-}	2.21e+00	2.21e+00	2.21e+00	2.21e+00	2.07e-01	2.21e+00
Si_6H_6	2.00e+02	1.86e+02	4.29e-01	2.00e+02	6.83e-01	1.81e+02
P_6	5.62e+02	5.30e+02	1.49e+00	7.76e-02	7.76e-02	7.76e-02
S_6	4.72e+02	1.42e+02	6.63e-01	1.12e-01	1.12e-01	1.12e-01
Ga_3^-	7.94e+00	1.03e+00	1.37e-01	6.32e-01	6.32e-01	6.32e-01
Ga_4^{2-}	1.32e+00	1.32e+00	1.32e+00	1.32e+00	8.72e-01	1.32e+00

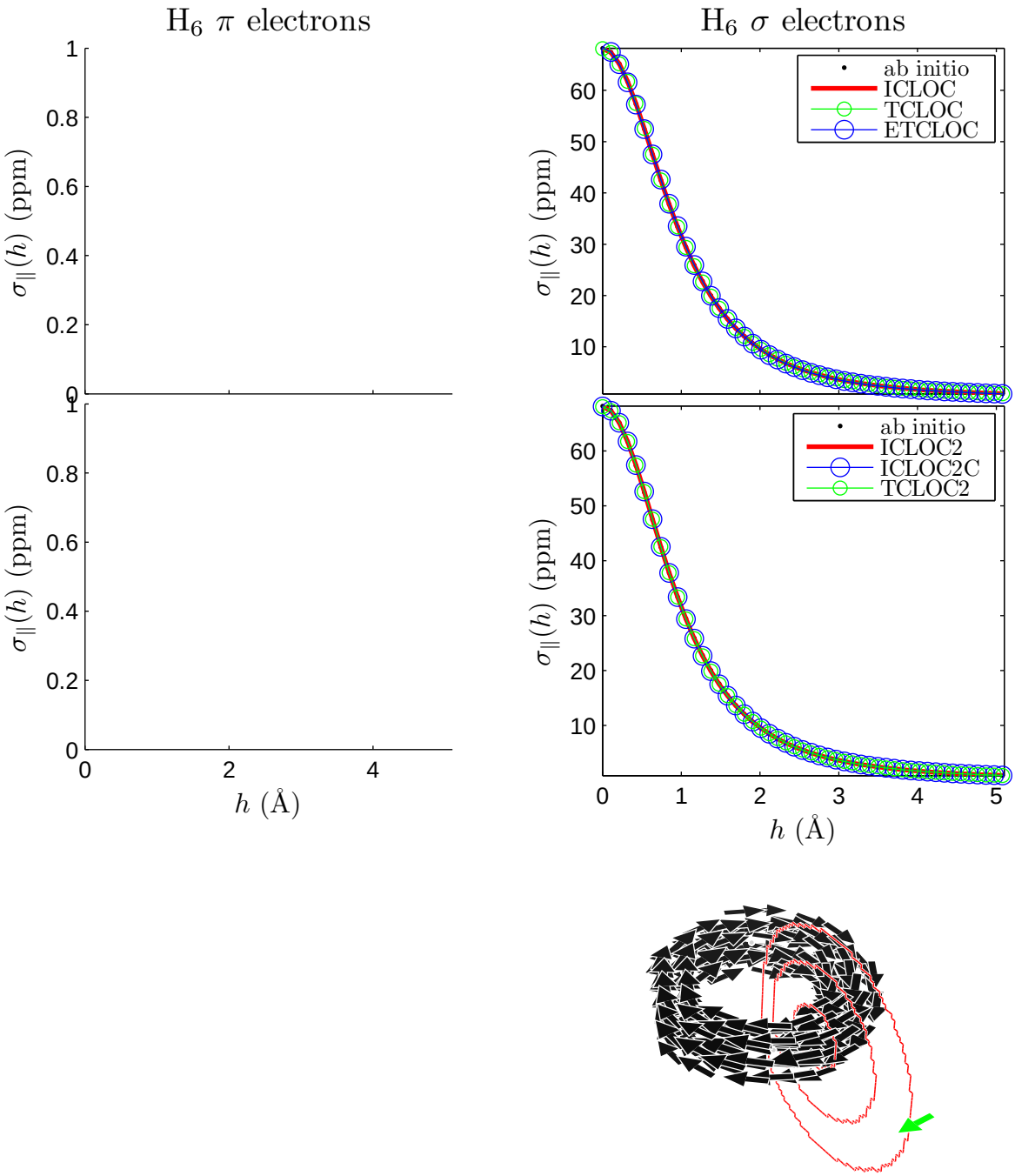

Figure 1: Scans of the contributions of π (top left) and σ (top right) electrons to the parallel component of magnetic shielding $\sigma_{\parallel} = -\mathrm{NICS}_{\parallel}$ computed *ab initio* and with different RCMs. On bottom the corresponding three-dimensional current density maps superposed on contour lines limiting domains D2, D16, D128 on the integration planes. The green arrow, corresponding to the maximum value of the π contribution to the current density in benzene (0.08 au) for a magnetic field perpendicular to the ring, is oriented in the diatropic sense. Definition of the domains and other graphical details as in Figure 2 of the Paper.

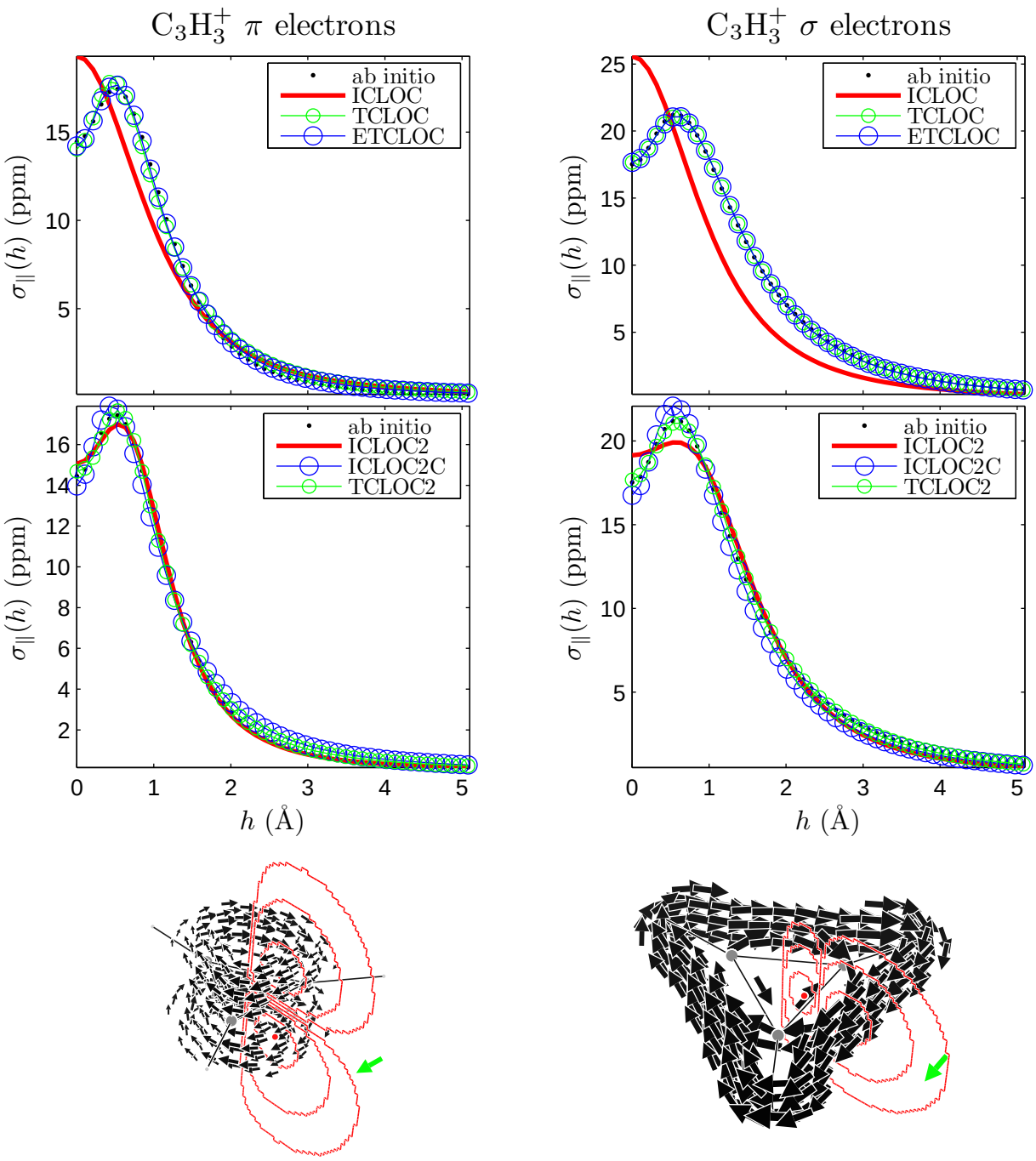

Figure 2: Scans of the contributions of π (top left) and σ (top right) electrons to the parallel component of magnetic shielding $\sigma_\parallel = -\mathrm{NICS}_\parallel$ computed *ab initio* and with different RCMs. On bottom the corresponding three-dimensional current density maps superposed on contour lines limiting domains D2, D16, D128 on the integration planes. The green arrow, corresponding to the maximum value of the π contribution to the current density in benzene (0.08 au) for a magnetic field perpendicular to the ring, is oriented in the diatropic sense. Definition of the domains and other graphical details as in Figure 2 of the Paper.

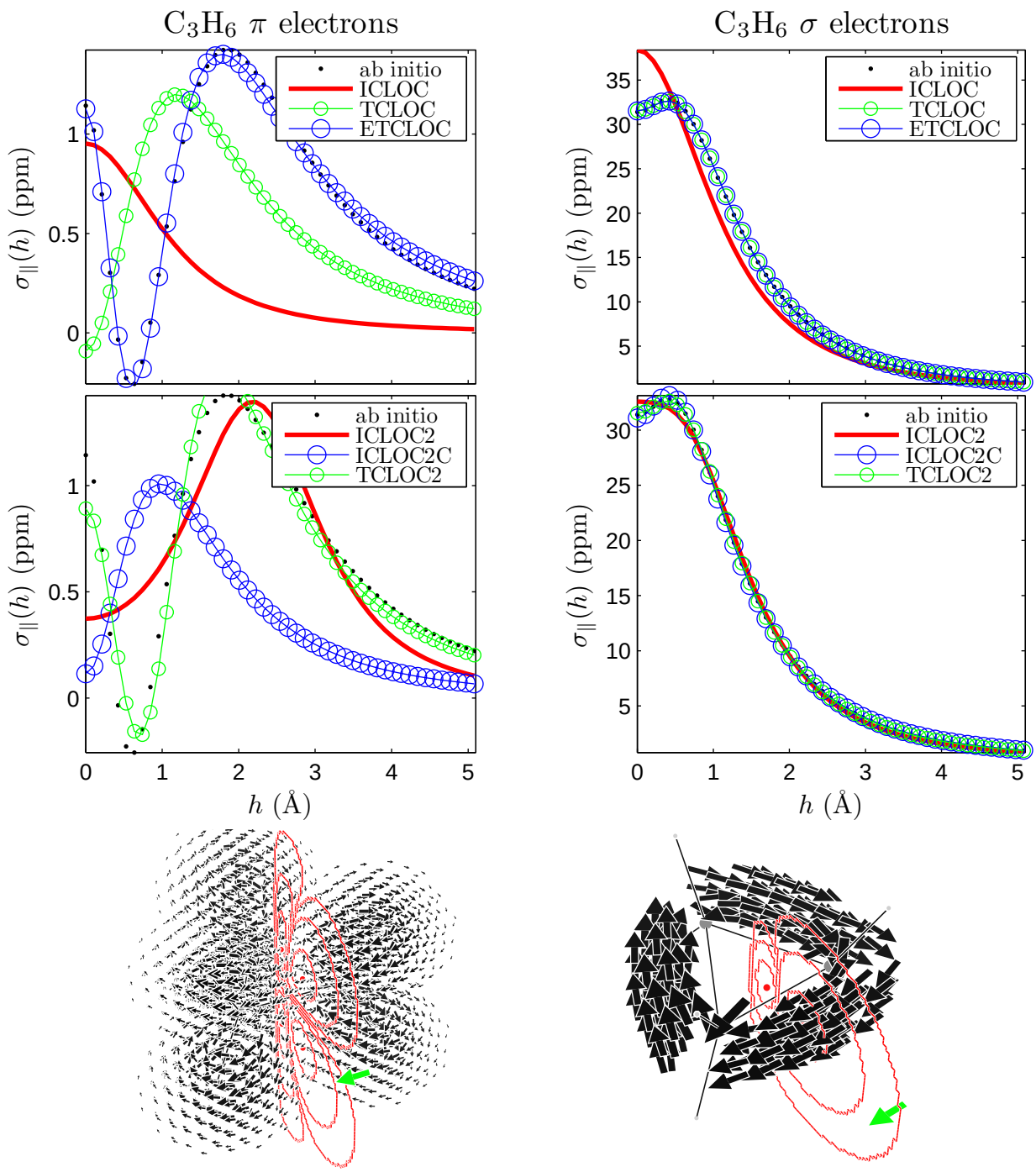

Figure 3: Scans of the contributions of π (top left) and σ (top right) electrons to the parallel component of magnetic shielding $\sigma_{\parallel} = -\mathrm{NICS}_{\parallel}$ computed *ab initio* and with different RCMs. On bottom the corresponding three-dimensional current density maps superposed on contour lines limiting domains D2, D16, D128 on the integration planes. The green arrow, corresponding to the maximum value of the π contribution to the current density in benzene (0.08 au) for a magnetic field perpendicular to the ring, is oriented in the diatropic sense. Definition of the domains and other graphical details as in Figure 2 of the Paper.

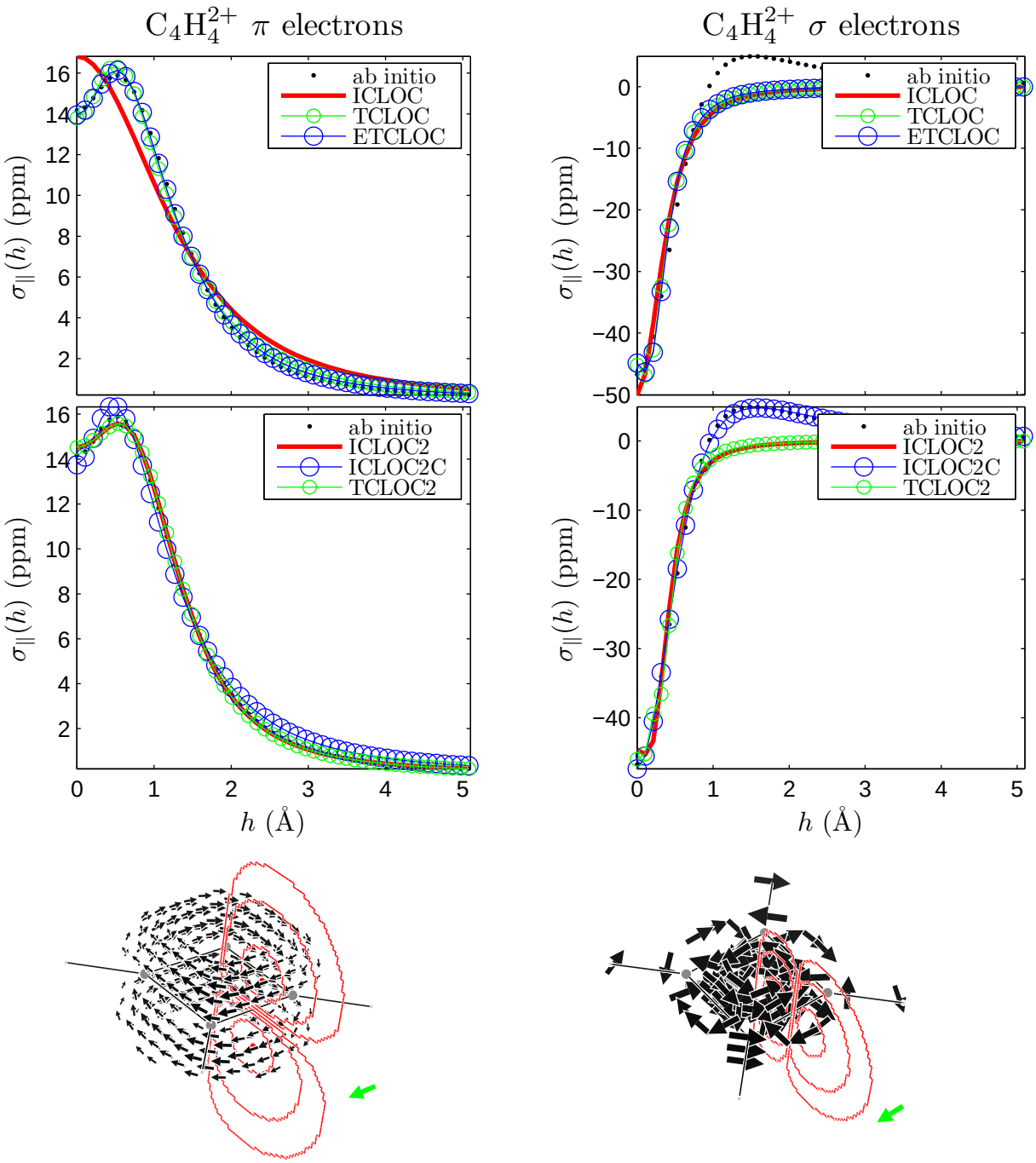

Figure 4: Scans of the contributions of π (top left) and σ (top right) electrons to the parallel component of magnetic shielding $\sigma_\parallel = -\mathrm{NICS}_\parallel$ computed *ab initio* and with different RCMs. On bottom the corresponding three-dimensional current density maps superposed on contour lines limiting domains D2, D16, D128 on the integration planes. The green arrow, corresponding to the maximum value of the π contribution to the current density in benzene (0.08 au) for a magnetic field perpendicular to the ring, is oriented in the diatropic sense. Definition of the domains and other graphical details as in Figure 2 of the Paper.

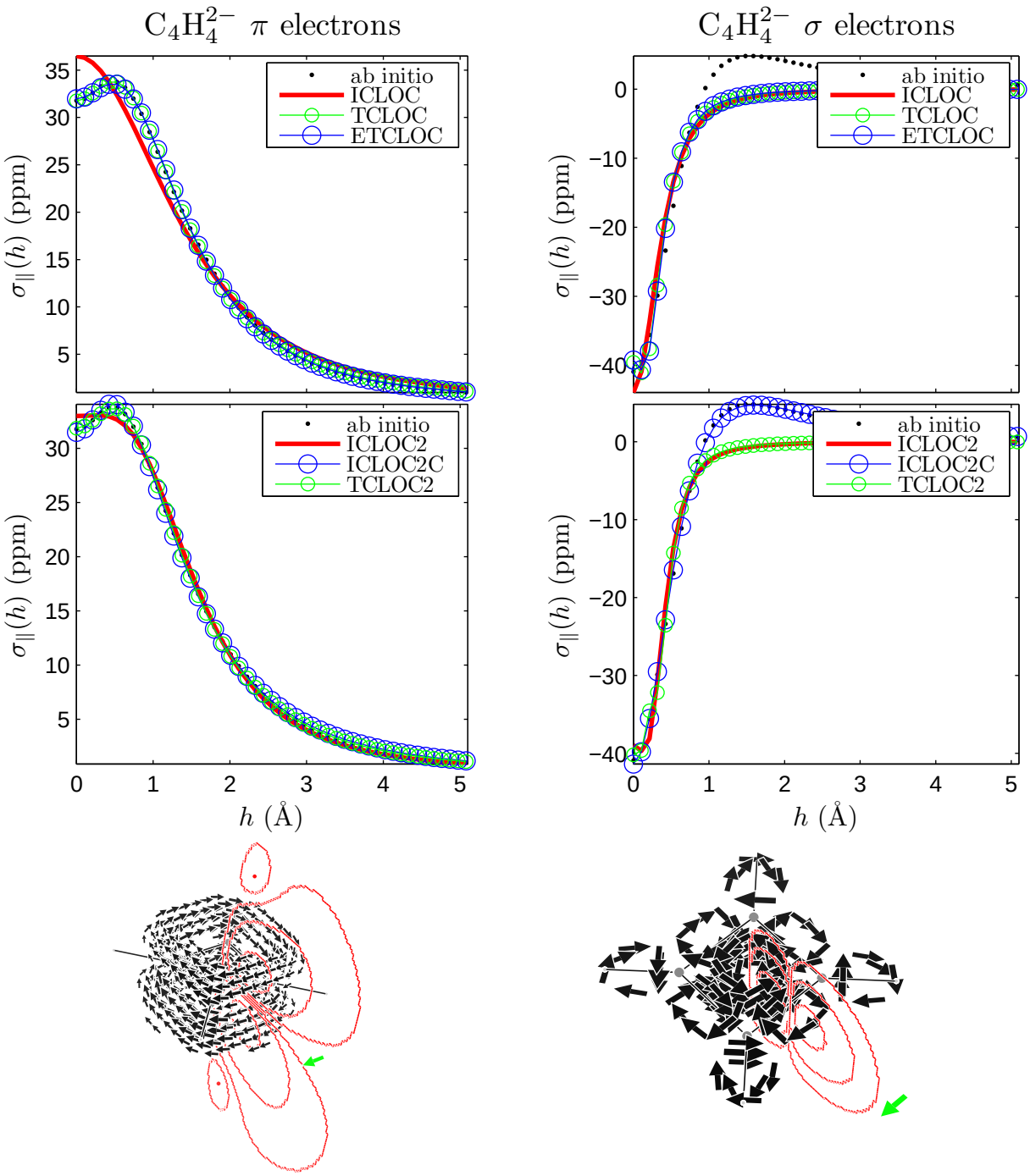

Figure 5: Scans of the contributions of π (top left) and σ (top right) electrons to the parallel component of magnetic shielding $\sigma_{\parallel} = -\mathrm{NICS}_{\parallel}$ computed *ab initio* and with different RCMs. On bottom the corresponding three-dimensional current density maps superposed on contour lines limiting domains D2, D16, D128 on the integration planes. The green arrow, corresponding to the maximum value of the π contribution to the current density in benzene (0.08 au) for a magnetic field perpendicular to the ring, is oriented in the diatropic sense. Definition of the domains and other graphical details as in Figure 2 of the Paper.

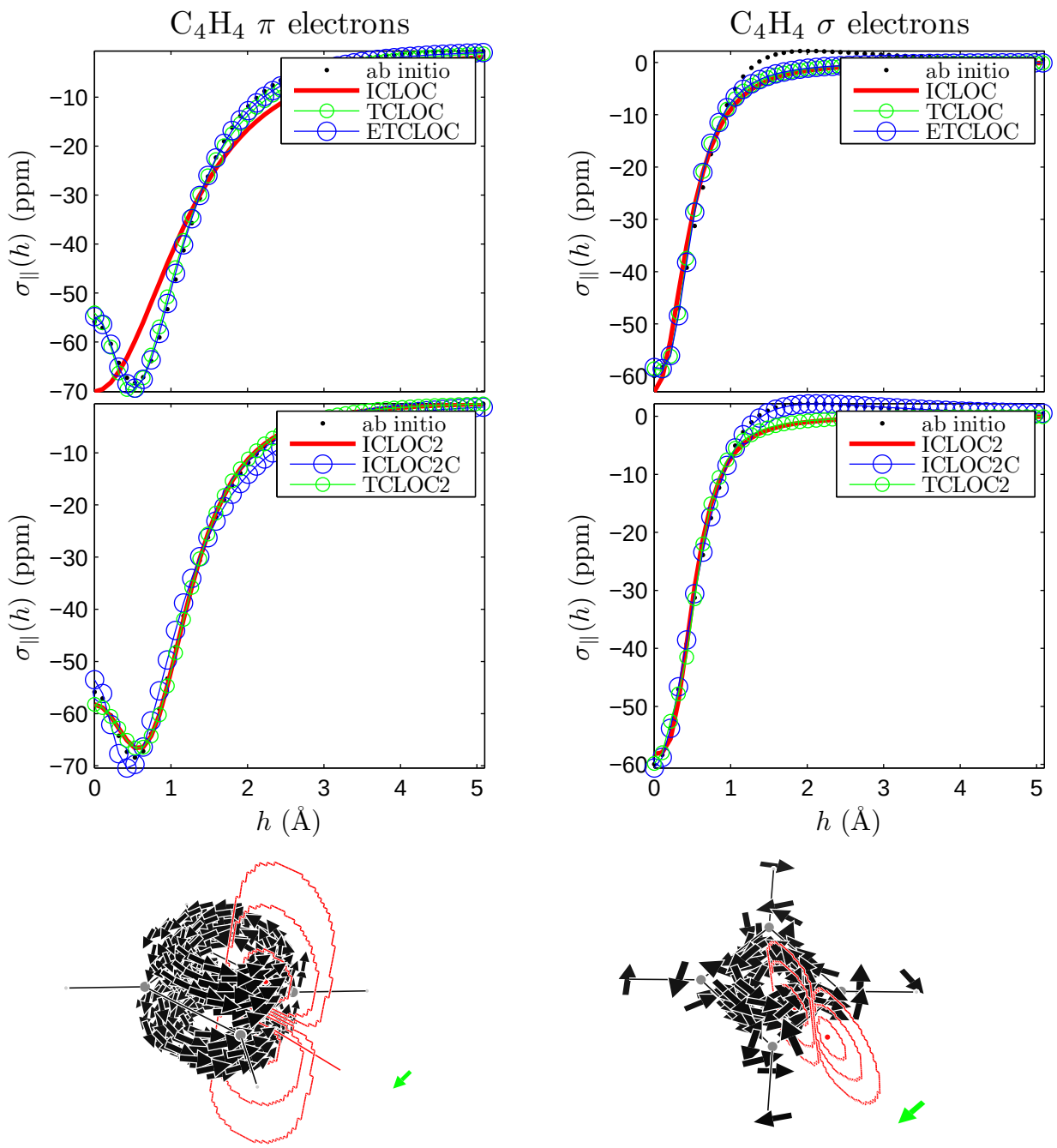

Figure 6: Scans of the contributions of π (top left) and σ (top right) electrons to the parallel component of magnetic shielding $\sigma_{\parallel} = -\mathrm{NICS}_{\parallel}$ computed *ab initio* and with different RCMs. On bottom the corresponding three-dimensional current density maps superposed on contour lines limiting domains D2, D16, D128 on the integration planes. The green arrow, corresponding to the maximum value of the π contribution to the current density in benzene (0.08 au) for a magnetic field perpendicular to the ring, is oriented in the diatropic sense. Definition of the domains and other graphical details as in Figure 2 of the Paper.

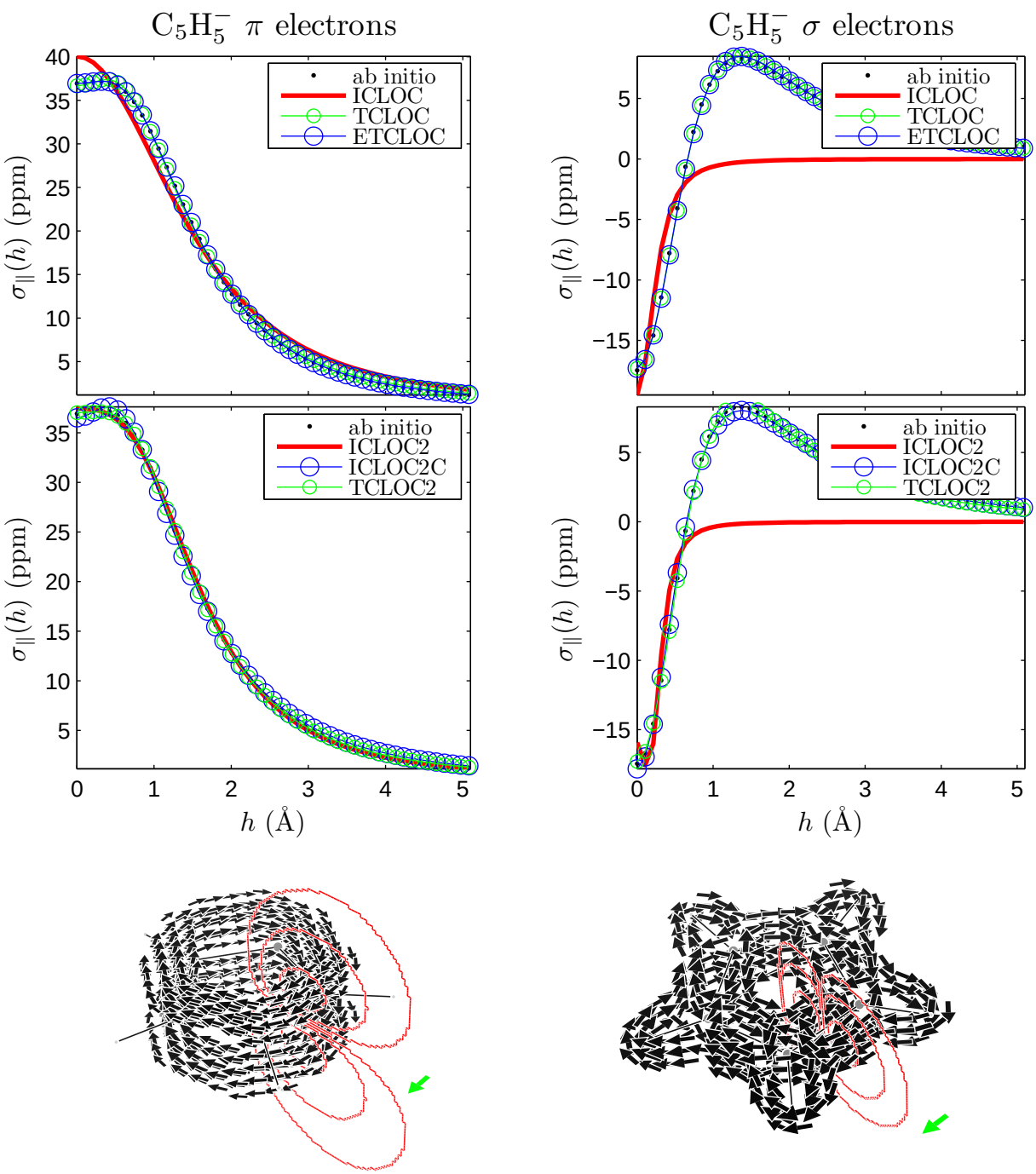

Figure 7: Scans of the contributions of π (top left) and σ (top right) electrons to the parallel component of magnetic shielding $\sigma_\parallel = -\mathrm{NICS}_\parallel$ computed *ab initio* and with different RCMs. On bottom the corresponding three-dimensional current density maps superposed on contour lines limiting domains D2, D16, D128 on the integration planes. The green arrow, corresponding to the maximum value of the π contribution to the current density in benzene (0.08 au) for a magnetic field perpendicular to the ring, is oriented in the diatropic sense. Definition of the domains and other graphical details as in Figure 2 of the Paper.

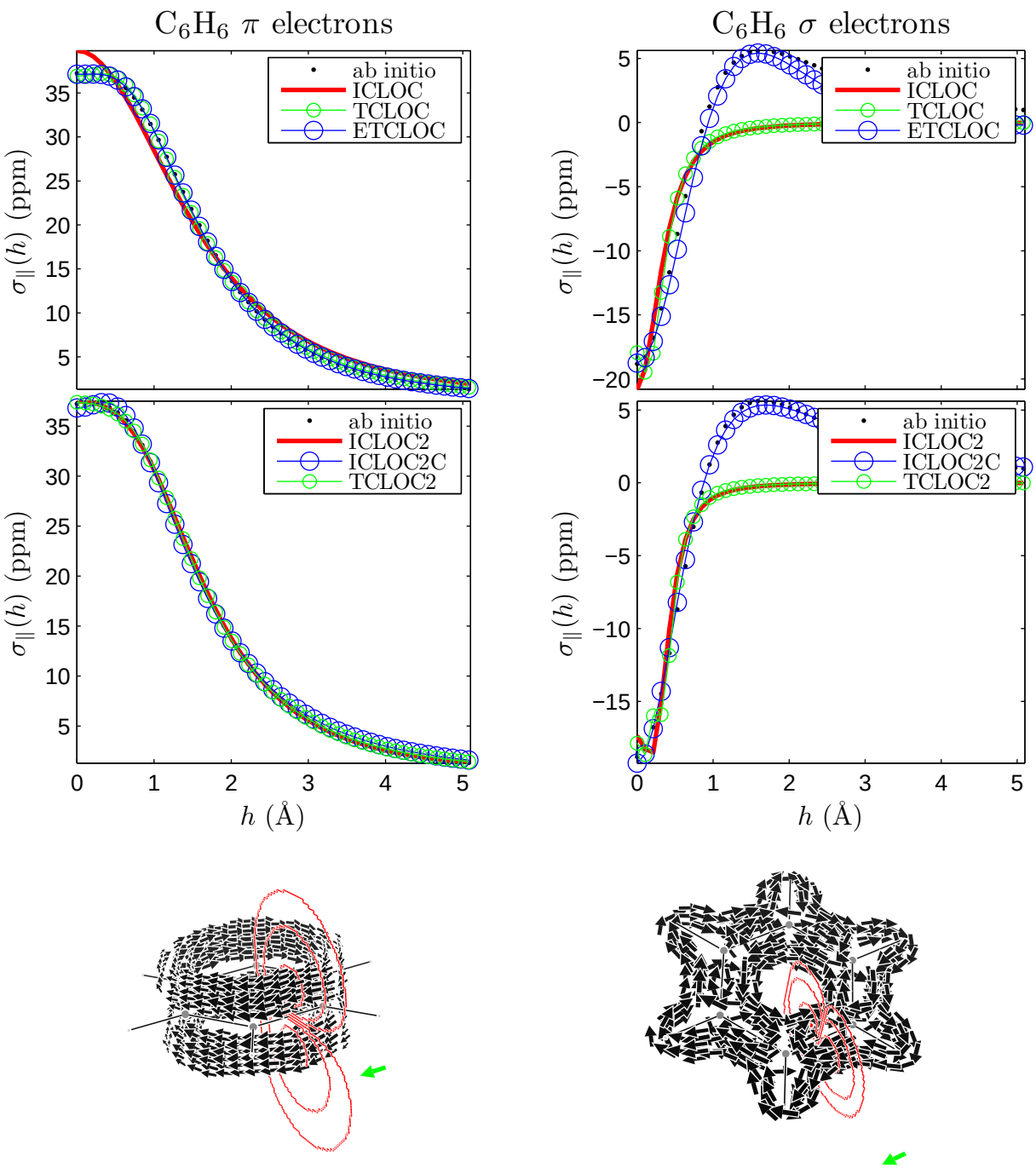

Figure 8: Scans of the contributions of π (top left) and σ (top right) electrons to the parallel component of magnetic shielding $\sigma_{\parallel} = -\mathrm{NICS}_{\parallel}$ computed *ab initio* and with different RCMs. On bottom the corresponding three-dimensional current density maps superposed on contour lines limiting domains D2, D16, D128 on the integration planes. The green arrow, corresponding to the maximum value of the π contribution to the current density in benzene (0.08 au) for a magnetic field perpendicular to the ring, is oriented in the diatropic sense. Definition of the domains and other graphical details as in Figure 2 of the Paper.

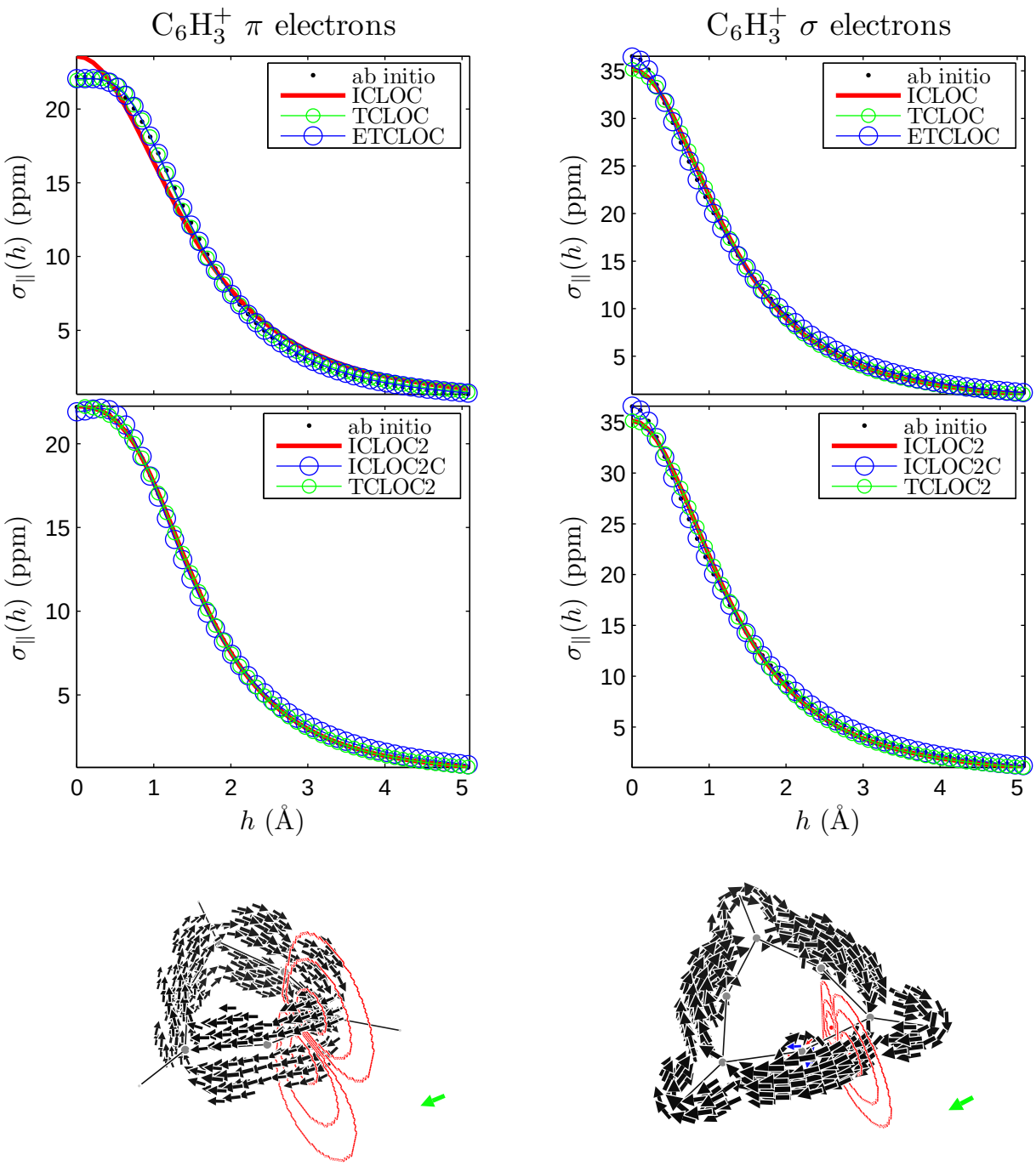

Figure 9: Scans of the contributions of π (top left) and σ (top right) electrons to the parallel component of magnetic shielding $\sigma_\parallel = -\mathrm{NICS}_\parallel$ computed *ab initio* and with different RCMs. On bottom the corresponding three-dimensional current density maps superposed on contour lines limiting domains D2, D16, D128 on the integration planes. The green arrow, corresponding to the maximum value of the π contribution to the current density in benzene (0.08 au) for a magnetic field perpendicular to the ring, is oriented in the diatropic sense. Definition of the domains and other graphical details as in Figure 2 of the Paper.

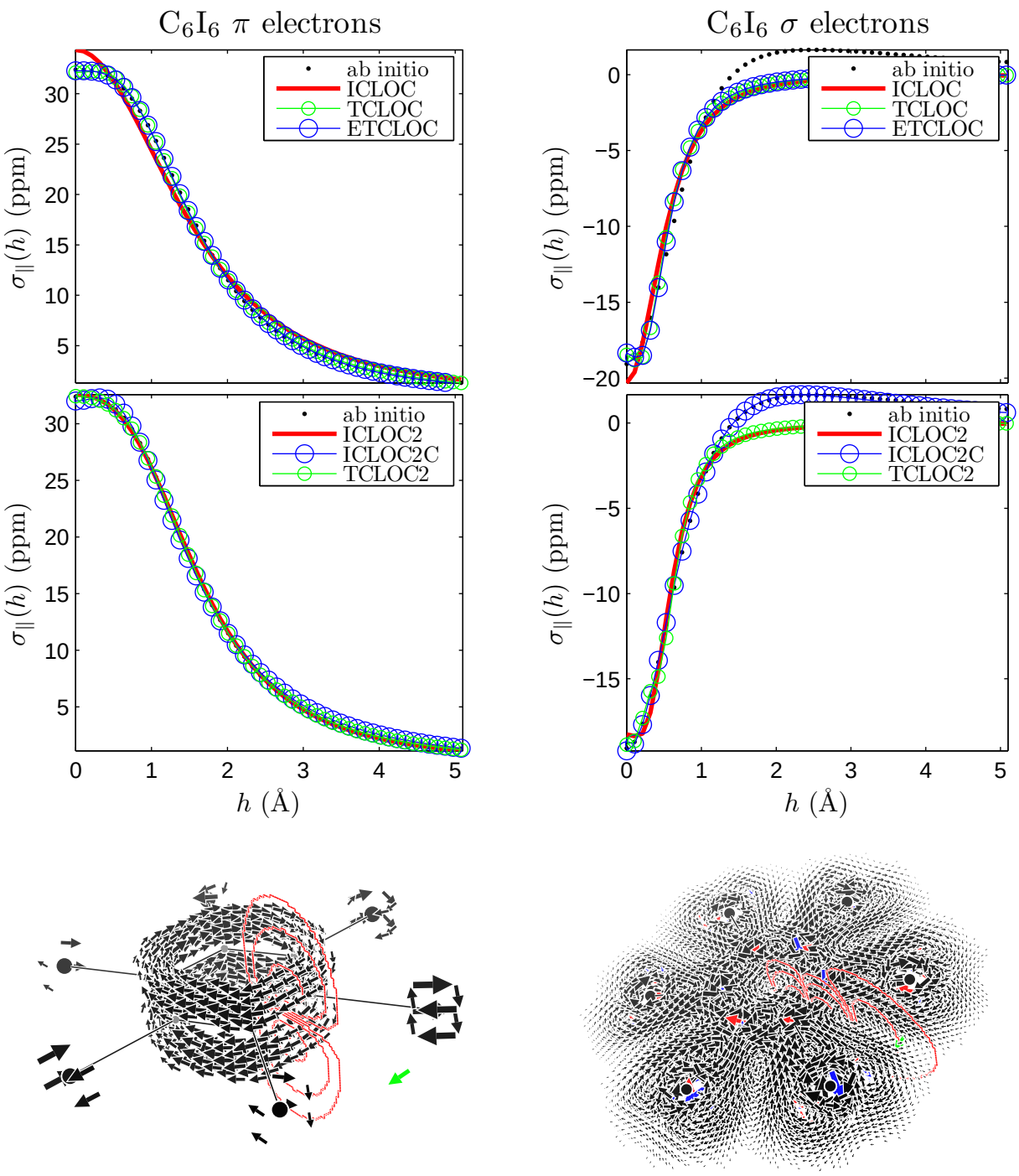

Figure 10: Scans of the contributions of π (top left) and σ (top right) electrons to the parallel component of magnetic shielding $\sigma_{\parallel} = -\mathrm{NICS}_{\parallel}$ computed *ab initio* and with different RCMs. On bottom the corresponding three-dimensional current density maps superposed on contour lines limiting domains D2, D16, D128 on the integration planes. The green arrow, corresponding to the maximum value of the π contribution to the current density in benzene (0.08 au) for a magnetic field perpendicular to the ring, is oriented in the diatropic sense. Definition of the domains and other graphical details as in Figure 2 of the Paper.

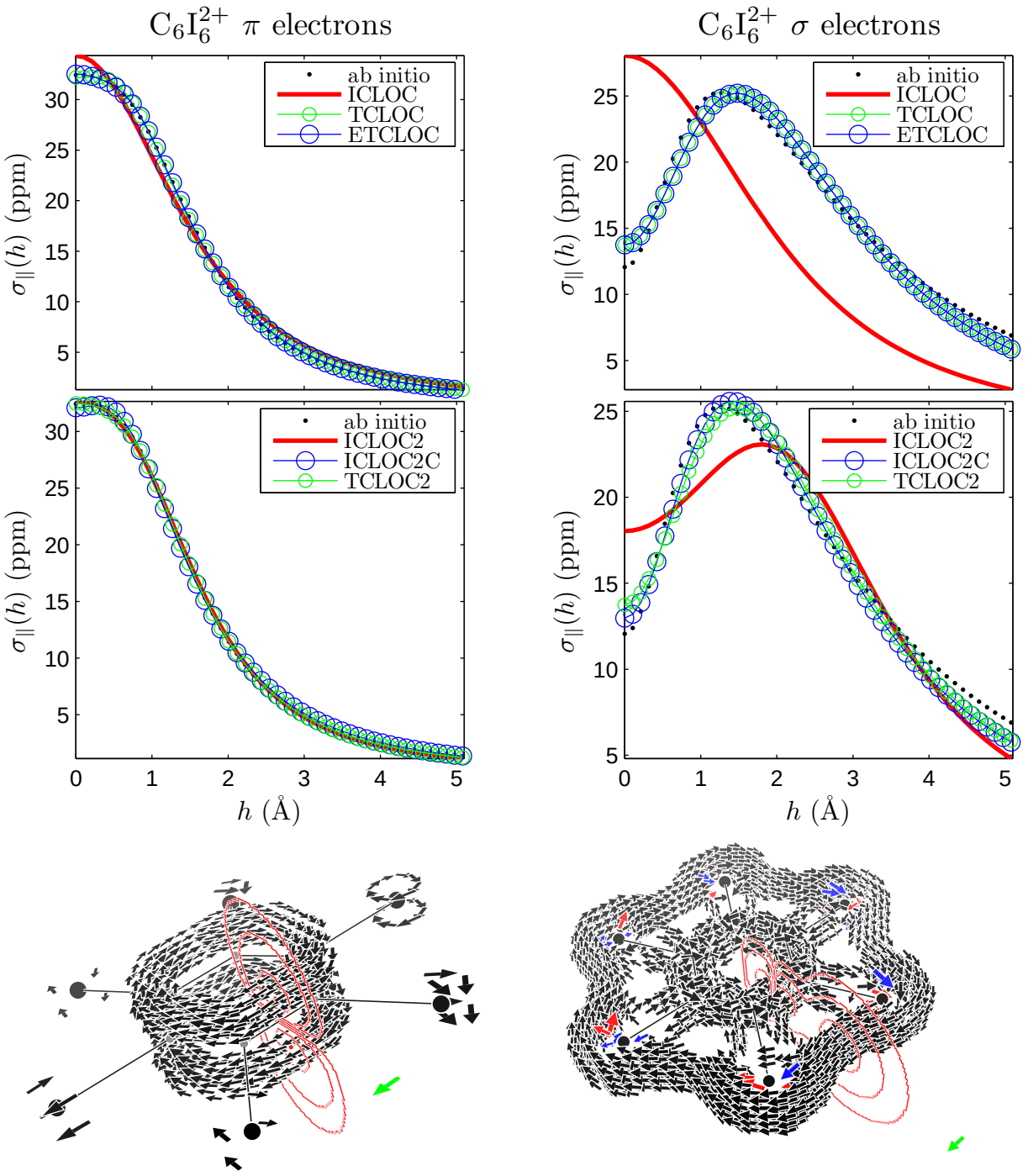

Figure 11: Scans of the contributions of π (top left) and σ (top right) electrons to the parallel component of magnetic shielding $\sigma_{\parallel} = -\mathrm{NICS}_{\parallel}$ computed *ab initio* and with different RCMs. On bottom the corresponding three-dimensional current density maps superposed on contour lines limiting domains D2, D16, D128 on the integration planes. The green arrow, corresponding to the maximum value of the π contribution to the current density in benzene (0.08 au) for a magnetic field perpendicular to the ring, is oriented in the diatropic sense. Definition of the domains and other graphical details as in Figure 2 of the Paper.

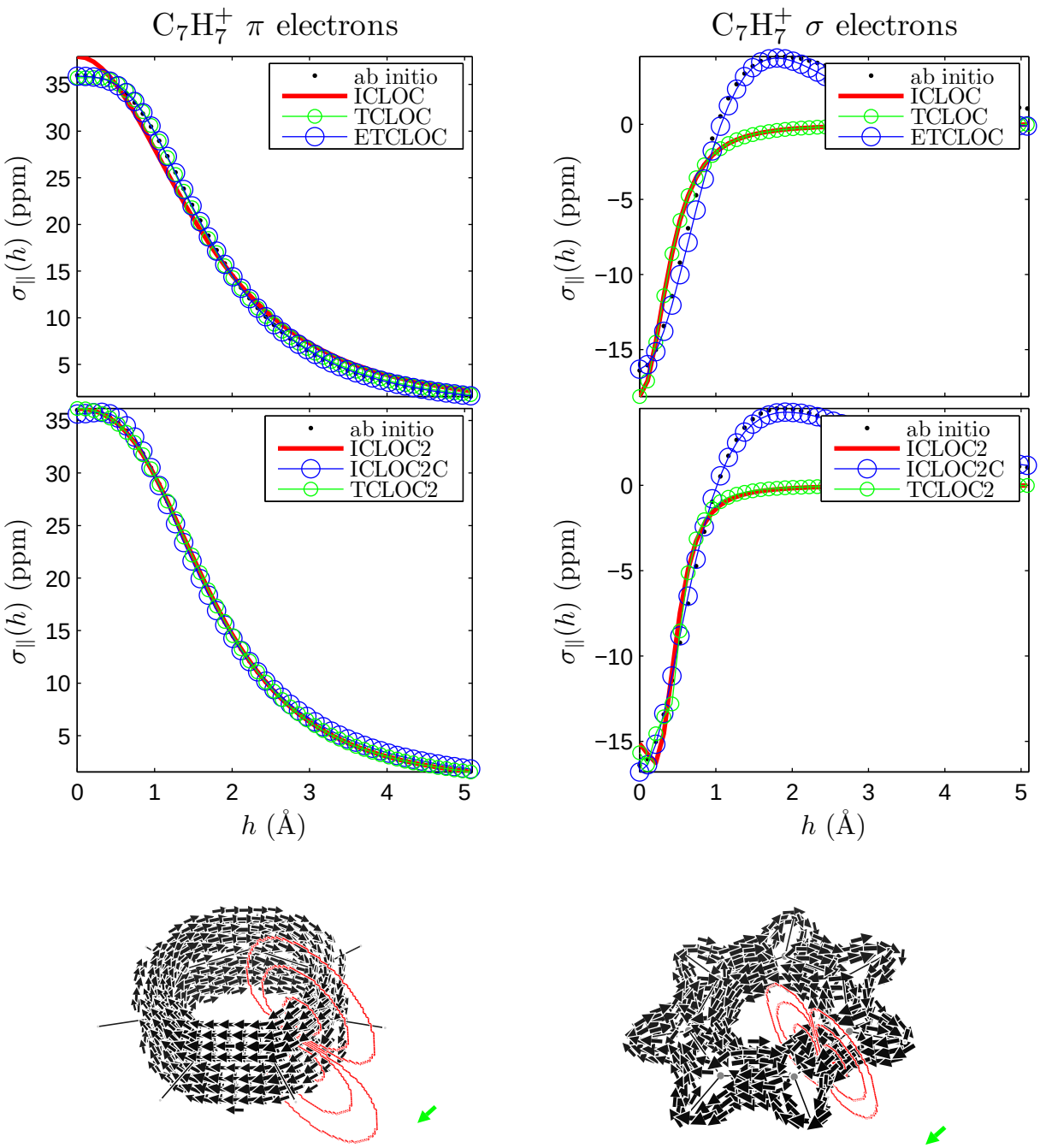

Figure 12: Scans of the contributions of π (top left) and σ (top right) electrons to the parallel component of magnetic shielding $\sigma_{\parallel} = -\mathrm{NICS}_{\parallel}$ computed *ab initio* and with different RCMs. On bottom the corresponding three-dimensional current density maps superposed on contour lines limiting domains D2, D16, D128 on the integration planes. The green arrow, corresponding to the maximum value of the π contribution to the current density in benzene (0.08 au) for a magnetic field perpendicular to the ring, is oriented in the diatropic sense. Definition of the domains and other graphical details as in Figure 2 of the Paper.

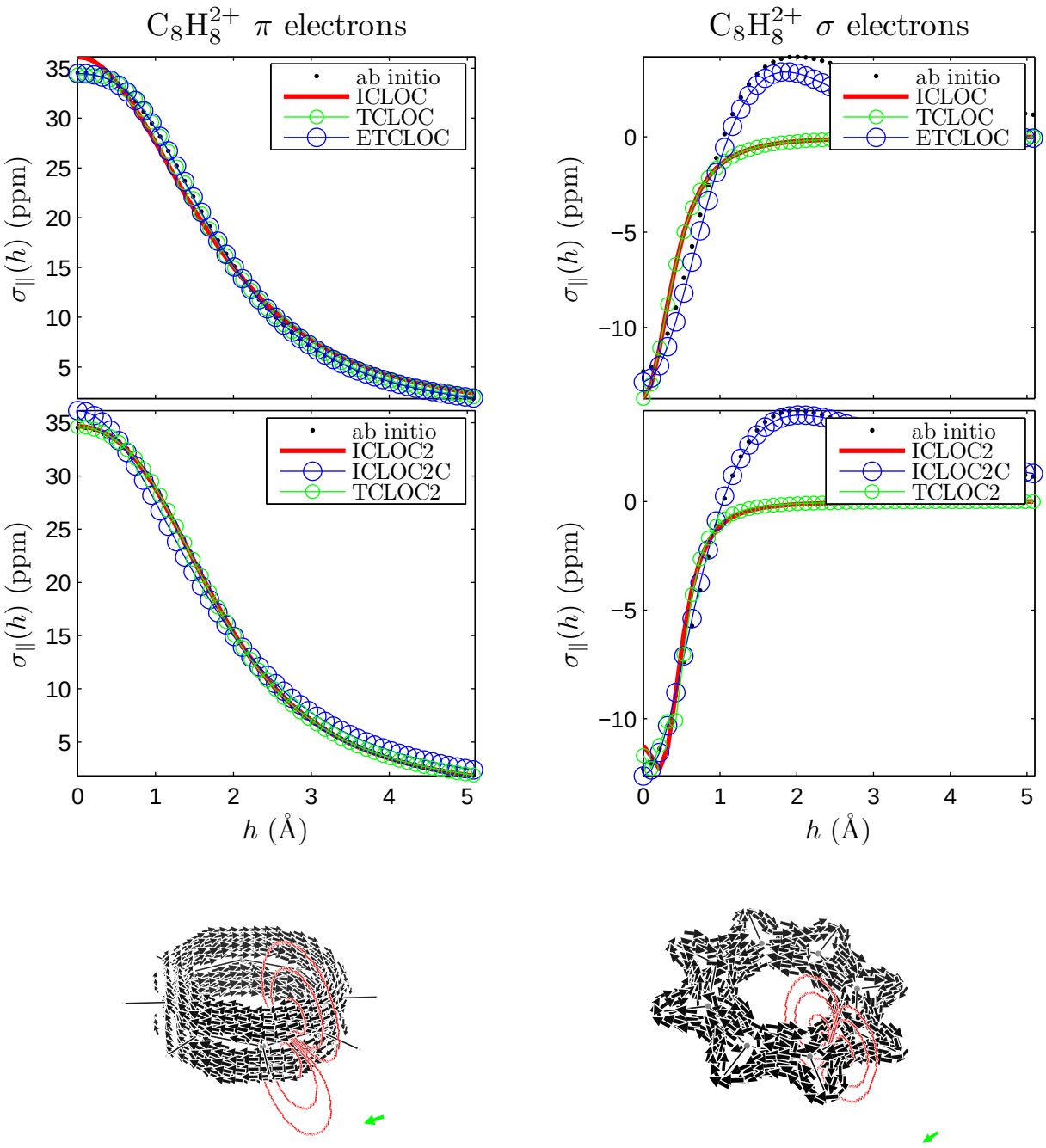

Figure 13: Scans of the contributions of π (top left) and σ (top right) electrons to the parallel component of magnetic shielding $\sigma_{\parallel} = -\mathrm{NICS}_{\parallel}$ computed *ab initio* and with different RCMs. On bottom the corresponding three-dimensional current density maps superposed on contour lines limiting domains D2, D16, D128 on the integration planes. The green arrow, corresponding to the maximum value of the π contribution to the current density in benzene (0.08 au) for a magnetic field perpendicular to the ring, is oriented in the diatropic sense. Definition of the domains and other graphical details as in Figure 2 of the Paper.

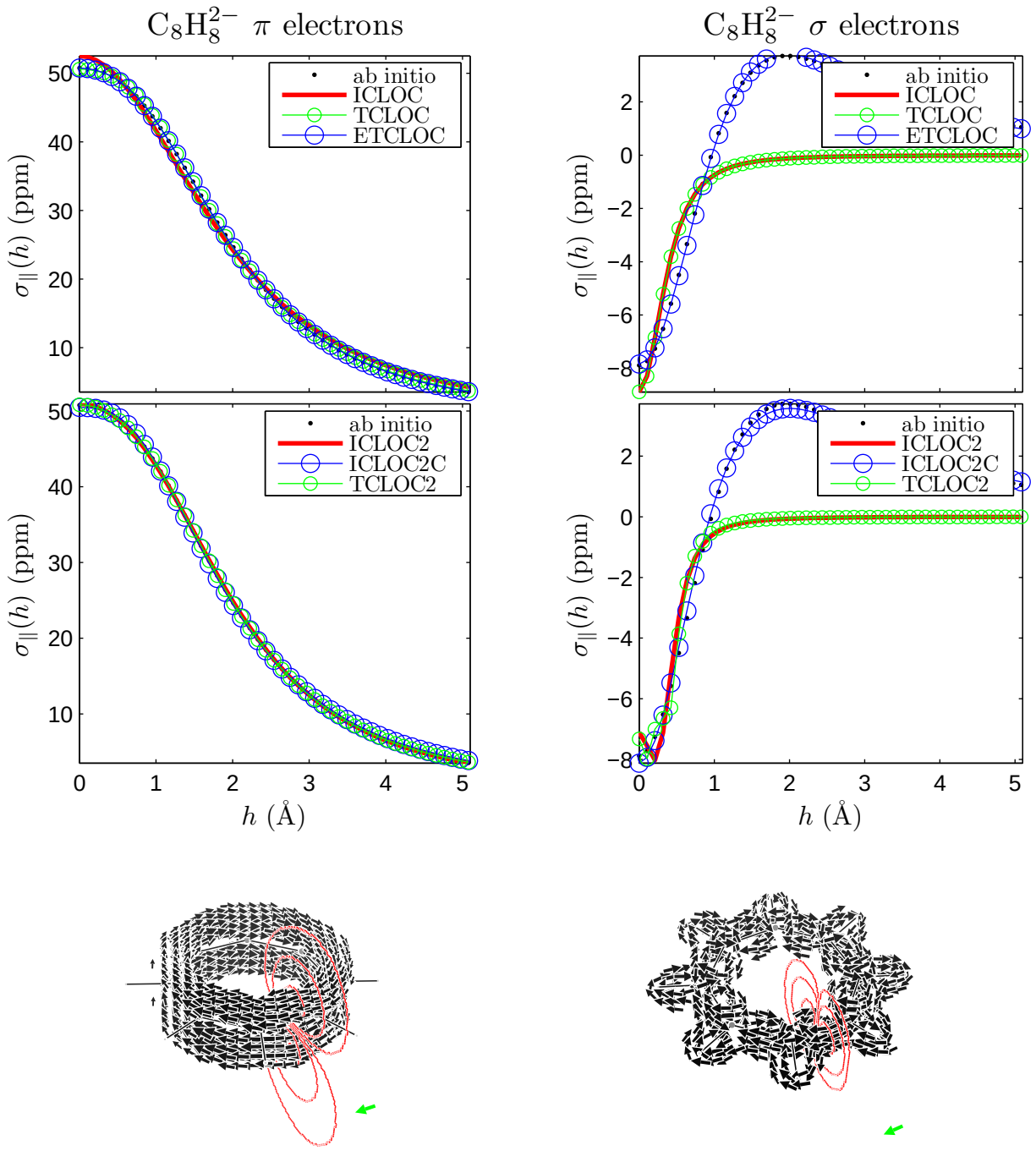

Figure 14: Scans of the contributions of π (top left) and σ (top right) electrons to the parallel component of magnetic shielding $\sigma_{\parallel} = -\mathrm{NICS}_{\parallel}$ computed *ab initio* and with different RCMs. On bottom the corresponding three-dimensional current density maps superposed on contour lines limiting domains D2, D16, D128 on the integration planes. The green arrow, corresponding to the maximum value of the π contribution to the current density in benzene (0.08 au) for a magnetic field perpendicular to the ring, is oriented in the diatropic sense. Definition of the domains and other graphical details as in Figure 2 of the Paper.

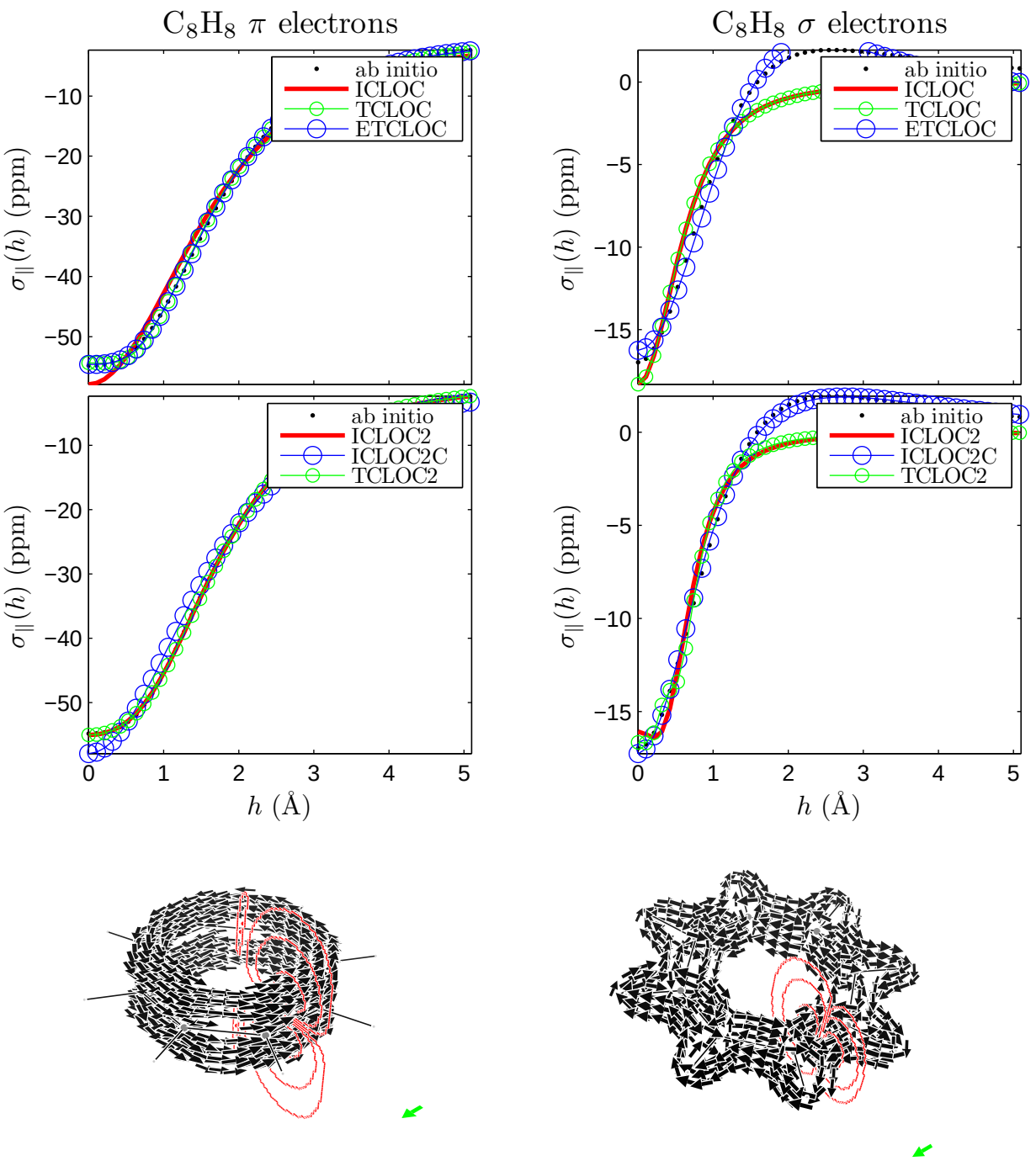

Figure 15: Scans of the contributions of π (top left) and σ (top right) electrons to the parallel component of magnetic shielding $\sigma_{\parallel} = -\mathrm{NICS}_{\parallel}$ computed *ab initio* and with different RCMs. On bottom the corresponding three-dimensional current density maps superposed on contour lines limiting domains D2, D16, D128 on the integration planes. The green arrow, corresponding to the maximum value of the π contribution to the current density in benzene (0.08 au) for a magnetic field perpendicular to the ring, is oriented in the diatropic sense. Definition of the domains and other graphical details as in Figure 2 of the Paper.

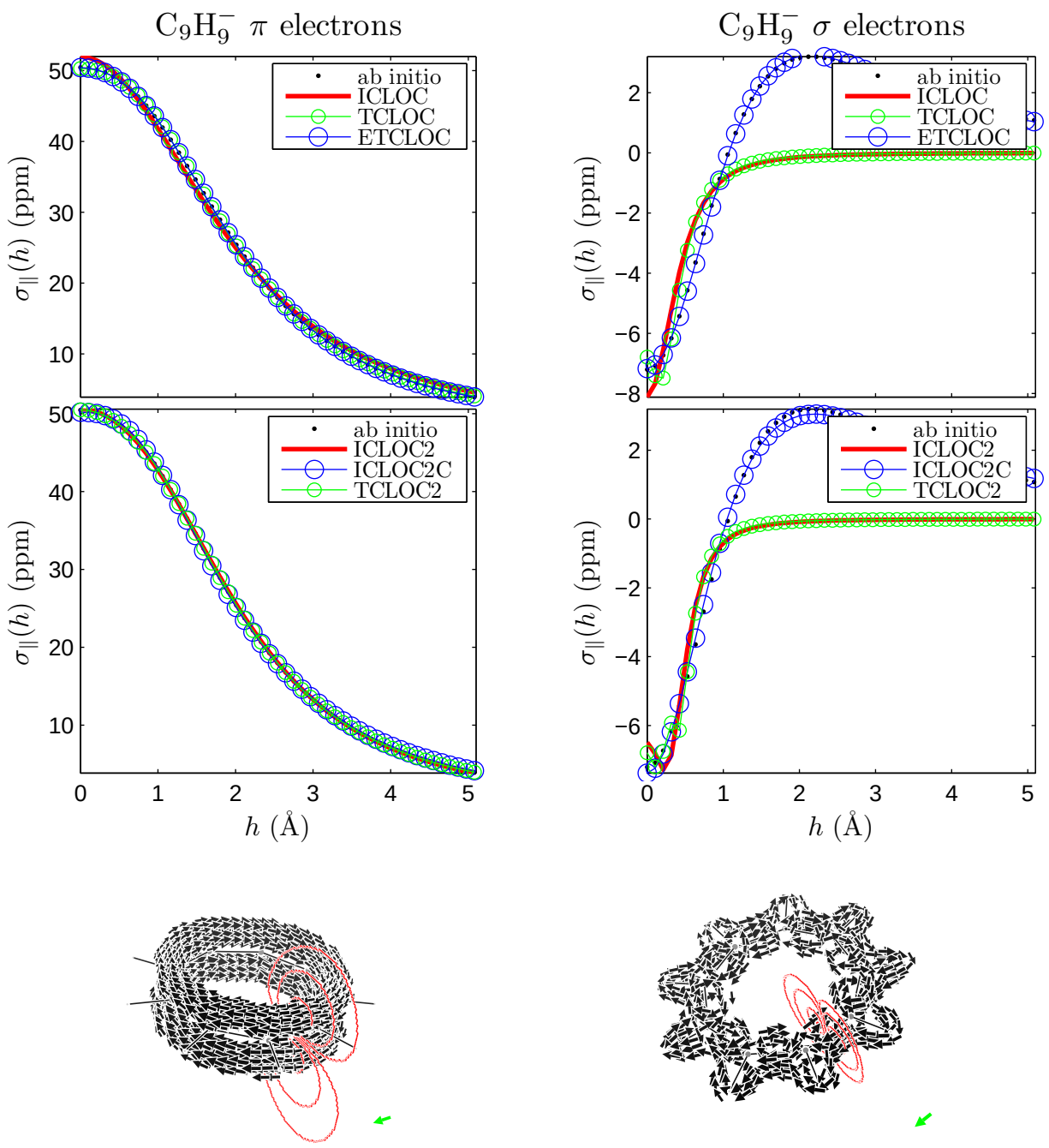

Figure 16: Scans of the contributions of π (top left) and σ (top right) electrons to the parallel component of magnetic shielding $\sigma_{\parallel} = -\mathrm{NICS}_{\parallel}$ computed *ab initio* and with different RCMs. On bottom the corresponding three-dimensional current density maps superposed on contour lines limiting domains D2, D16, D128 on the integration planes. The green arrow, corresponding to the maximum value of the π contribution to the current density in benzene (0.08 au) for a magnetic field perpendicular to the ring, is oriented in the diatropic sense. Definition of the domains and other graphical details as in Figure 2 of the Paper.

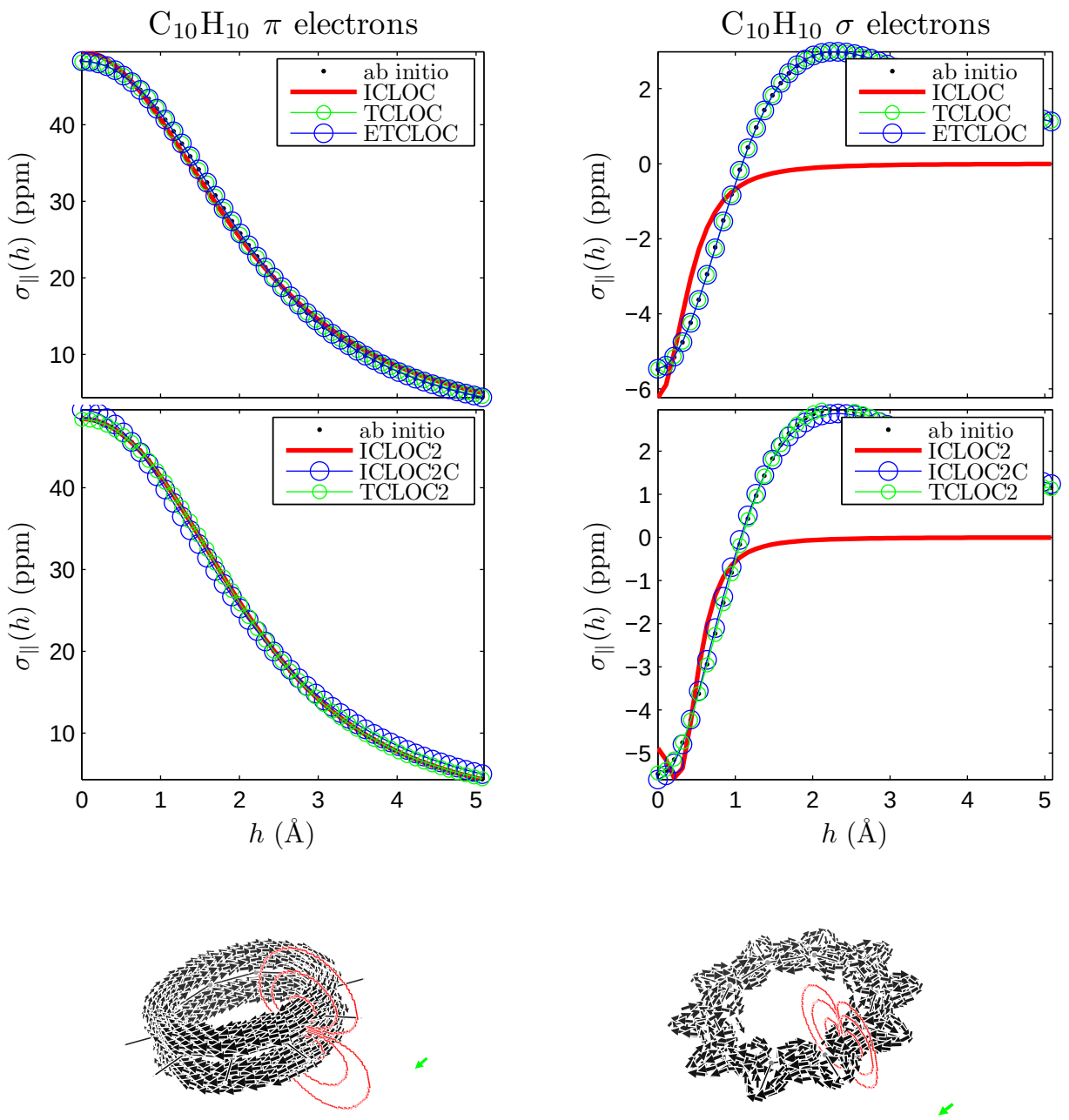

Figure 17: Scans of the contributions of π (top left) and σ (top right) electrons to the parallel component of magnetic shielding $\sigma_{\parallel} = -\mathrm{NICS}_{\parallel}$ computed *ab initio* and with different RCMs. On bottom the corresponding three-dimensional current density maps superposed on contour lines limiting domains D2, D16, D128 on the integration planes. The green arrow, corresponding to the maximum value of the π contribution to the current density in benzene (0.08 au) for a magnetic field perpendicular to the ring, is oriented in the diatropic sense. Definition of the domains and other graphical details as in Figure 2 of the Paper.

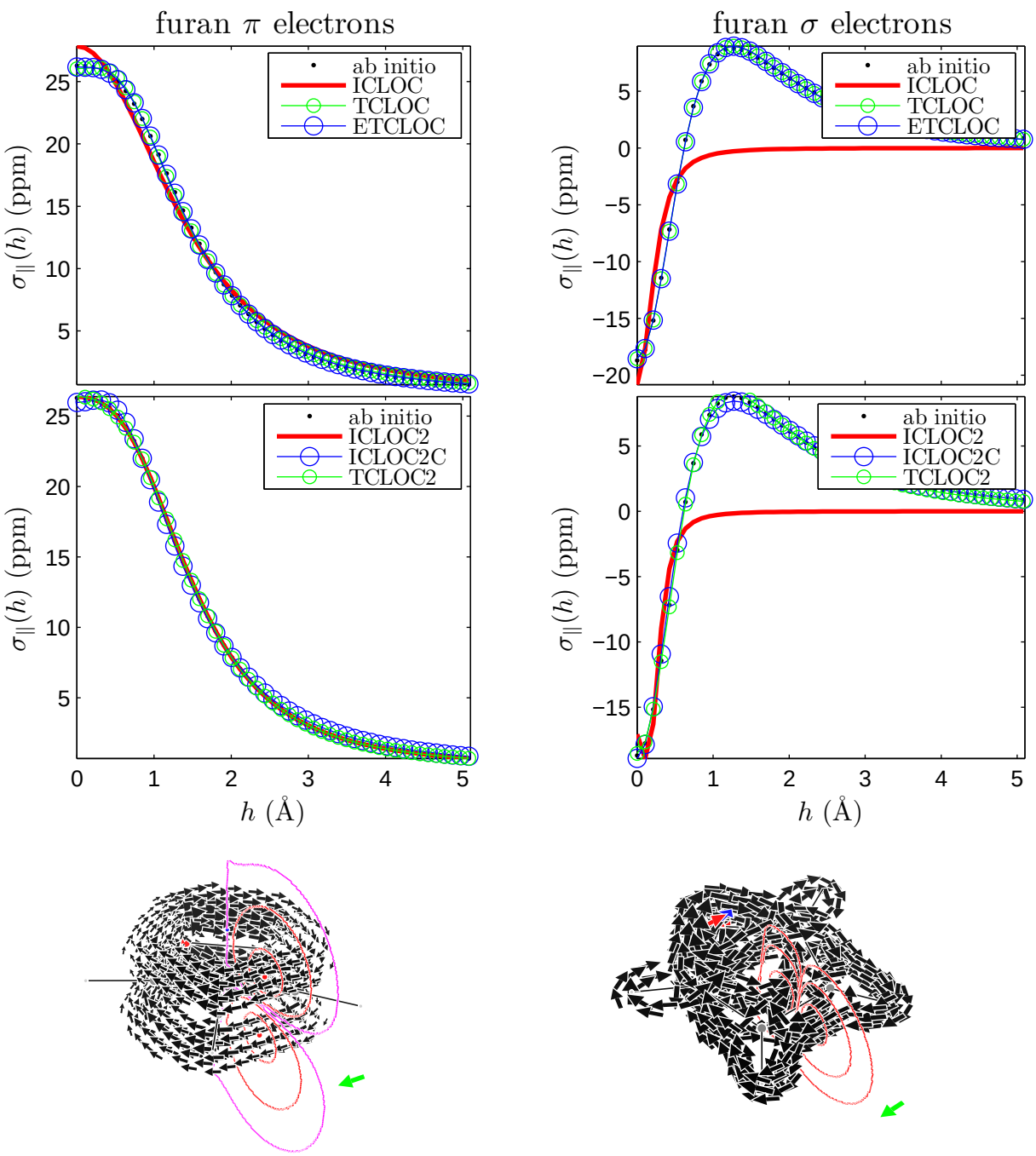

Figure 18: Scans of the contributions of π (top left) and σ (top right) electrons to the parallel component of magnetic shielding $\sigma_{\parallel} = -\mathrm{NICS}_{\parallel}$ computed *ab initio* and with different RCMs. On bottom the corresponding three-dimensional current density maps superposed on contour lines limiting domains D2, D16, D128 on the integration planes. The green arrow, corresponding to the maximum value of the π contribution to the current density in benzene (0.08 au) for a magnetic field perpendicular to the ring, is oriented in the diatropic sense. Definition of the domains and other graphical details as in Figure 2 of the Paper.

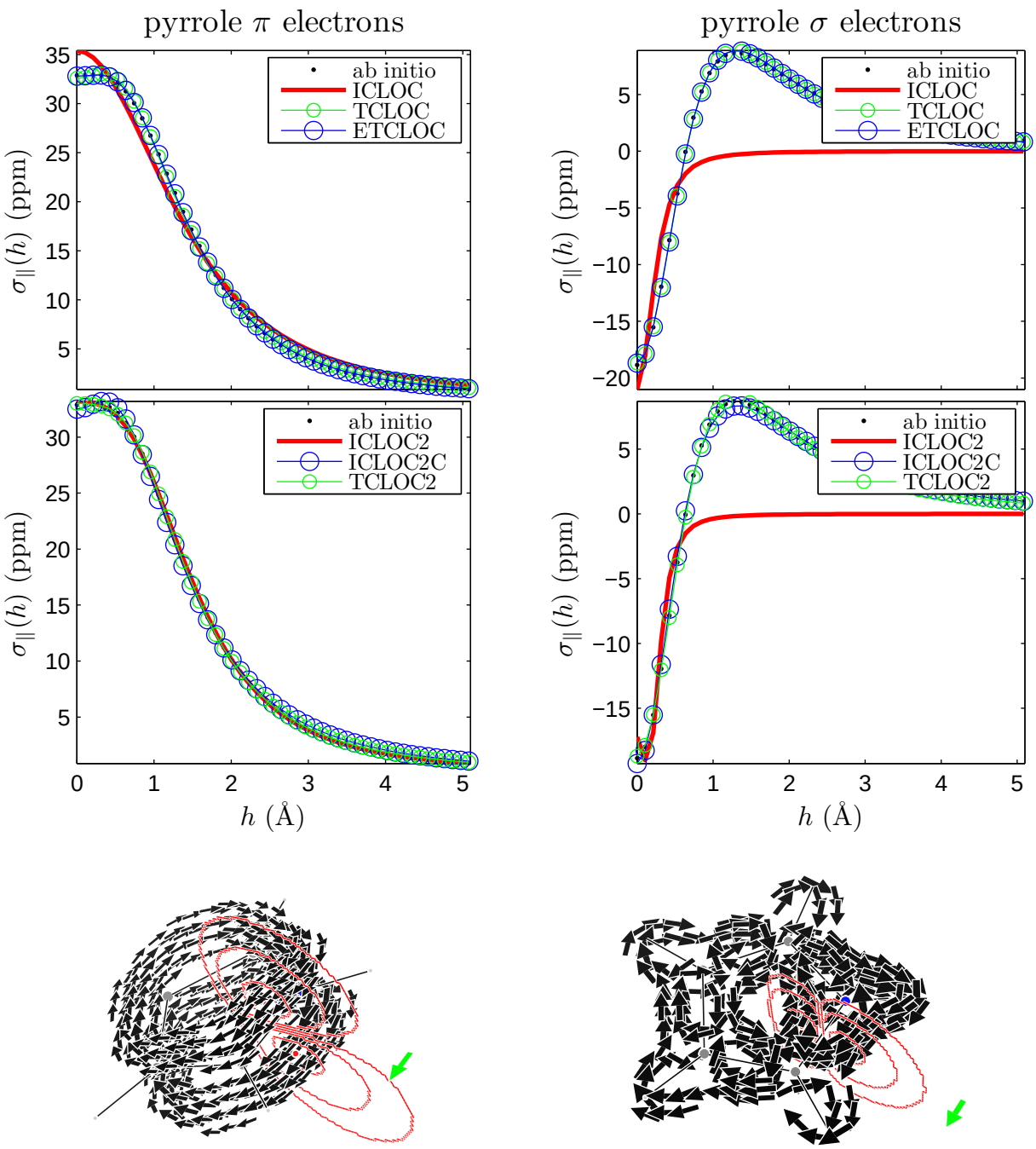

Figure 19: Scans of the contributions of π (top left) and σ (top right) electrons to the parallel component of magnetic shielding $\sigma_{\parallel} = -\mathrm{NICS}_{\parallel}$ computed *ab initio* and with different RCMs. On bottom the corresponding three-dimensional current density maps superposed on contour lines limiting domains D2, D16, D128 on the integration planes. The green arrow, corresponding to the maximum value of the π contribution to the current density in benzene (0.08 au) for a magnetic field perpendicular to the ring, is oriented in the diatropic sense. Definition of the domains and other graphical details as in Figure 2 of the Paper.

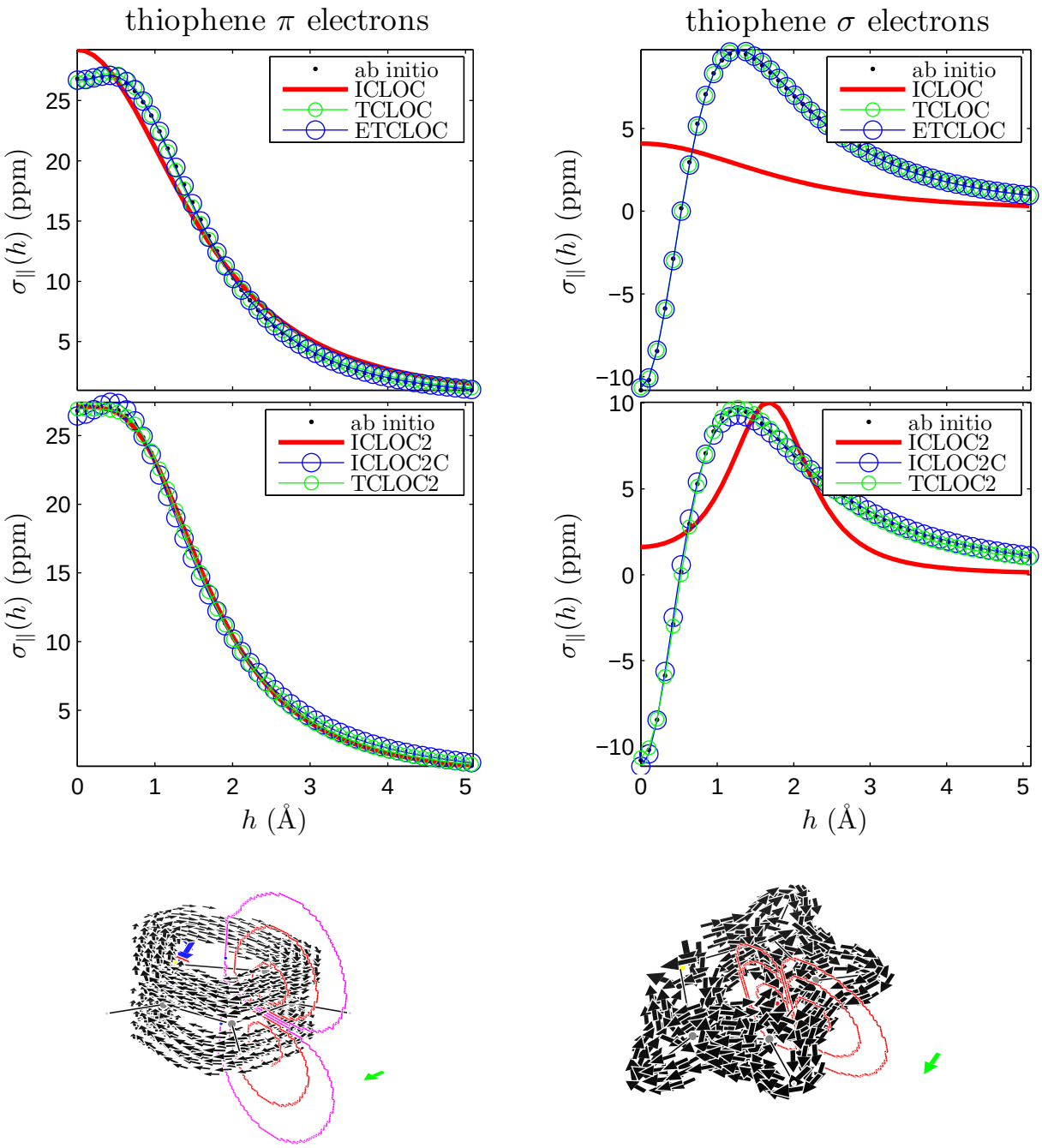

Figure 20: Scans of the contributions of π (top left) and σ (top right) electrons to the parallel component of magnetic shielding $\sigma_{\parallel} = -\mathrm{NICS}_{\parallel}$ computed *ab initio* and with different RCMs. On bottom the corresponding three-dimensional current density maps superposed on contour lines limiting domains D2, D16, D128 on the integration planes. The green arrow, corresponding to the maximum value of the π contribution to the current density in benzene (0.08 au) for a magnetic field perpendicular to the ring, is oriented in the diatropic sense. Definition of the domains and other graphical details as in Figure 2 of the Paper.

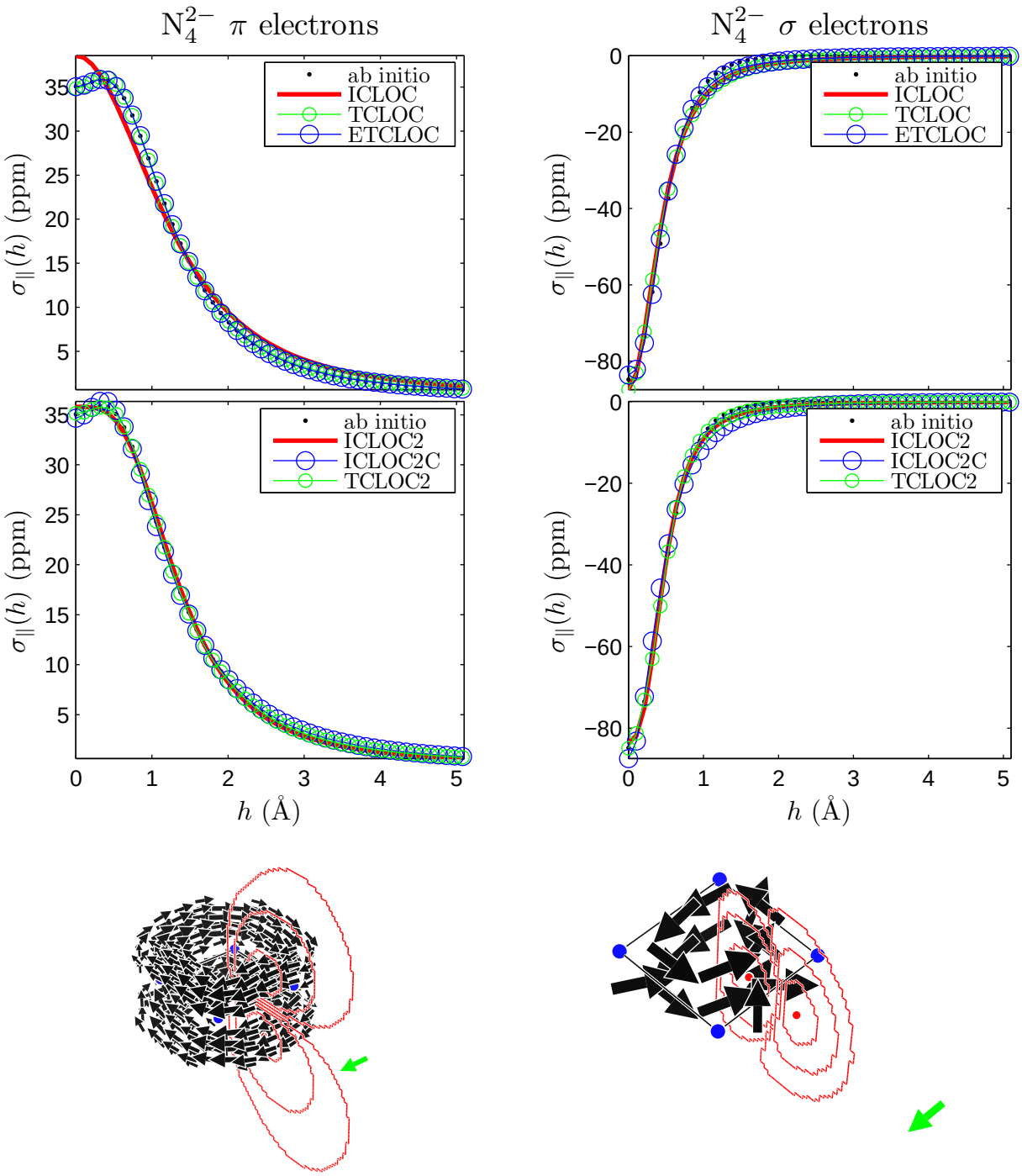

Figure 21: Scans of the contributions of π (top left) and σ (top right) electrons to the parallel component of magnetic shielding $\sigma_{\parallel} = -\mathrm{NICS}_{\parallel}$ computed *ab initio* and with different RCMs. On bottom the corresponding three-dimensional current density maps superposed on contour lines limiting domains D2, D16, D128 on the integration planes. The green arrow, corresponding to the maximum value of the π contribution to the current density in benzene (0.08 au) for a magnetic field perpendicular to the ring, is oriented in the diatropic sense. Definition of the domains and other graphical details as in Figure 2 of the Paper.

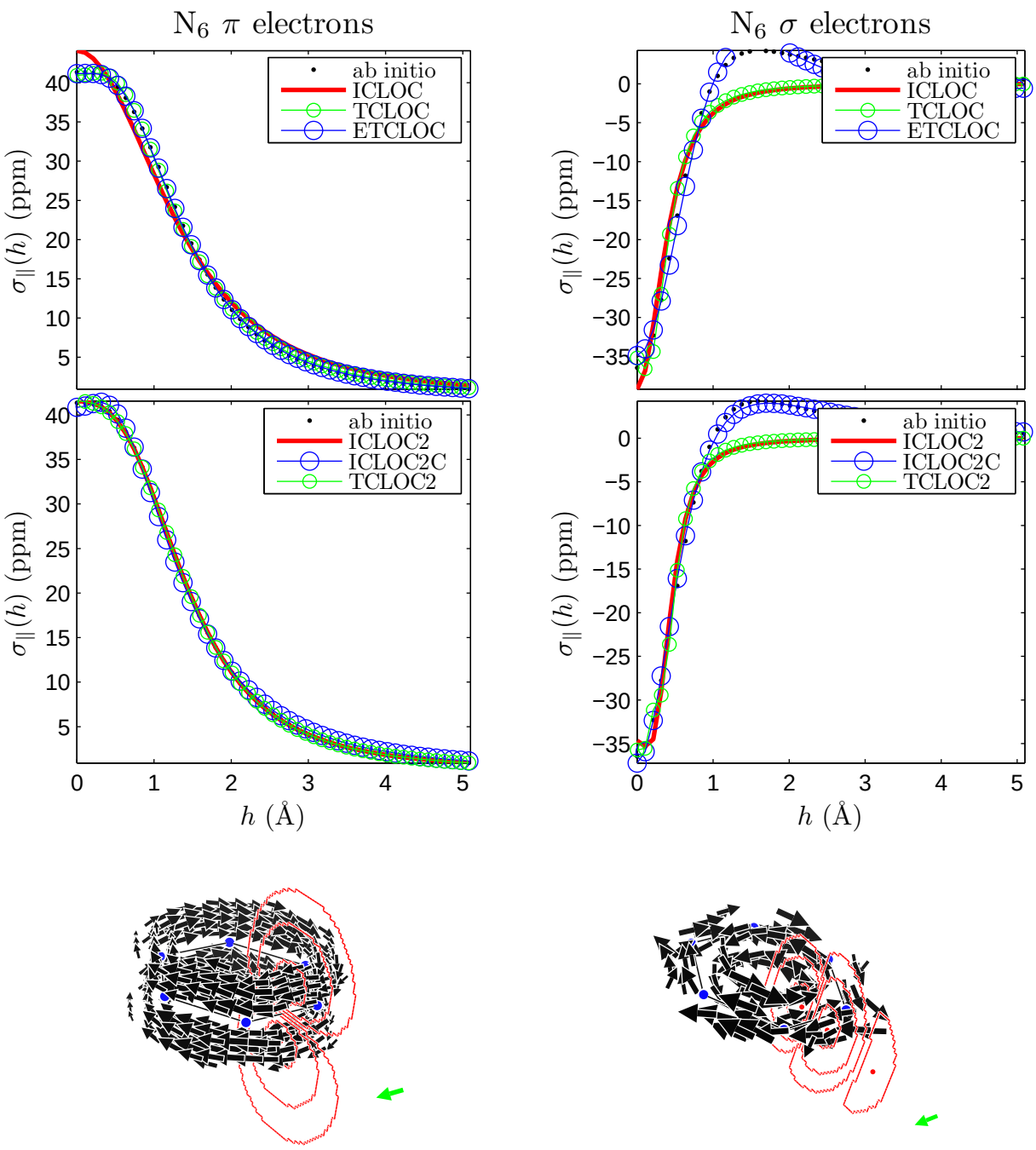

Figure 22: Scans of the contributions of π (top left) and σ (top right) electrons to the parallel component of magnetic shielding $\sigma_{\parallel} = -\mathrm{NICS}_{\parallel}$ computed *ab initio* and with different RCMs. On bottom the corresponding three-dimensional current density maps superposed on contour lines limiting domains D2, D16, D128 on the integration planes. The green arrow, corresponding to the maximum value of the π contribution to the current density in benzene (0.08 au) for a magnetic field perpendicular to the ring, is oriented in the diatropic sense. Definition of the domains and other graphical details as in Figure 2 of the Paper.

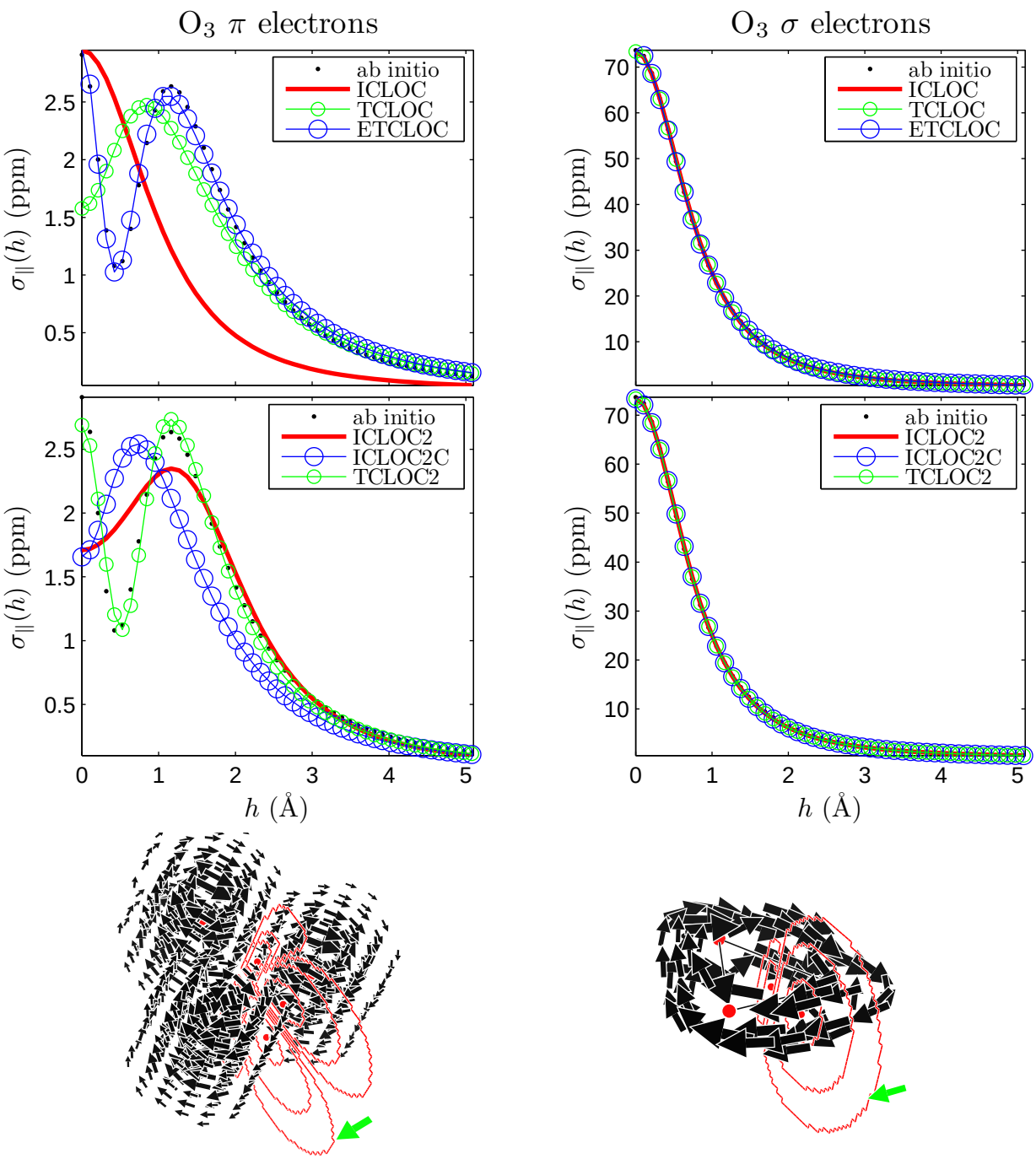

Figure 23: Scans of the contributions of π (top left) and σ (top right) electrons to the parallel component of magnetic shielding $\sigma_{\parallel} = -\mathrm{NICS}_{\parallel}$ computed *ab initio* and with different RCMs. On bottom the corresponding three-dimensional current density maps superposed on contour lines limiting domains D2, D16, D128 on the integration planes. The green arrow, corresponding to the maximum value of the π contribution to the current density in benzene (0.08 au) for a magnetic field perpendicular to the ring, is oriented in the diatropic sense. Definition of the domains and other graphical details as in Figure 2 of the Paper.

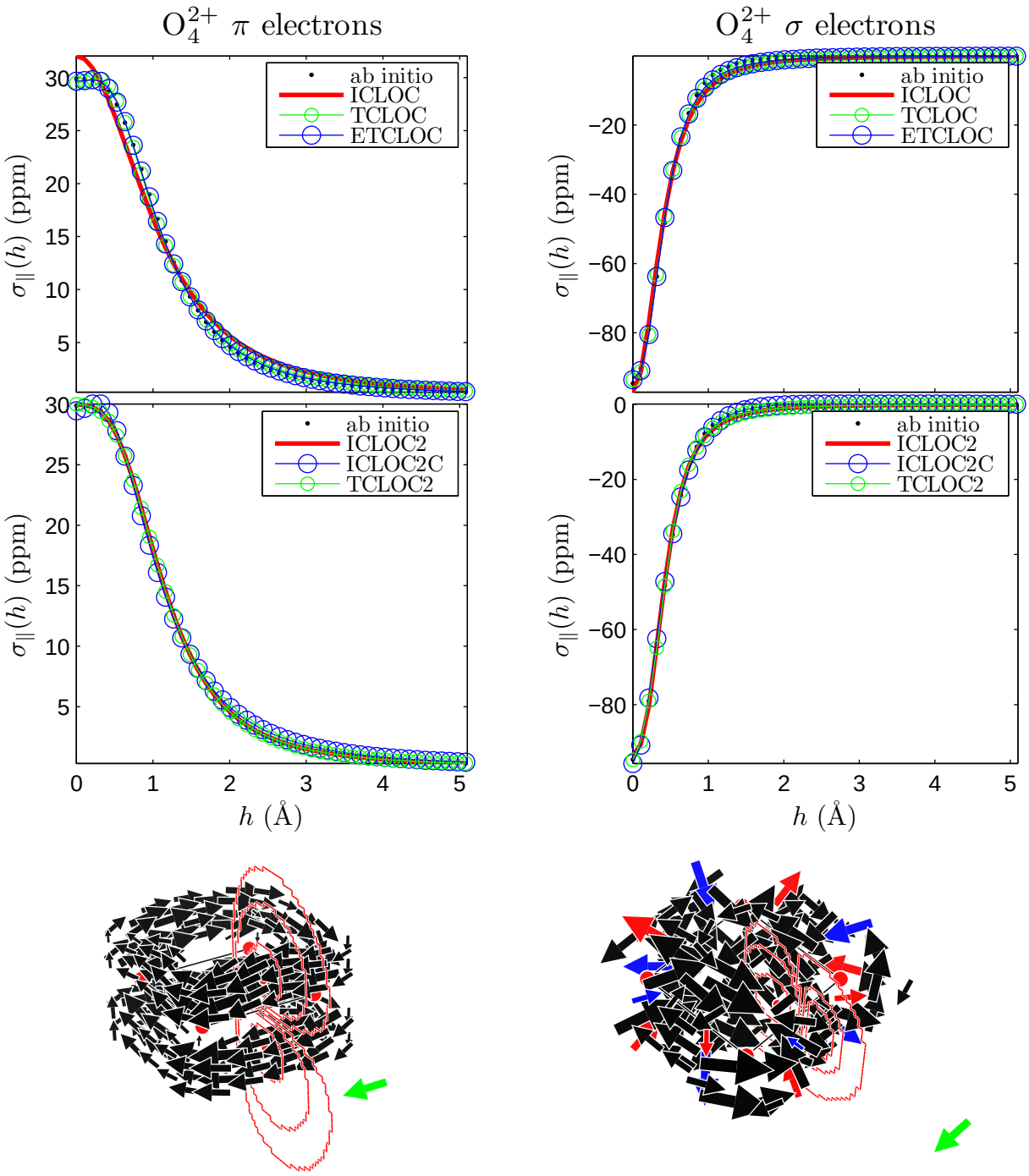

Figure 24: Scans of the contributions of π (top left) and σ (top right) electrons to the parallel component of magnetic shielding $\sigma_{\parallel} = -\mathrm{NICS}_{\parallel}$ computed *ab initio* and with different RCMs. On bottom the corresponding three-dimensional current density maps superposed on contour lines limiting domains D2, D16, D128 on the integration planes. The green arrow, corresponding to the maximum value of the π contribution to the current density in benzene (0.08 au) for a magnetic field perpendicular to the ring, is oriented in the diatropic sense. Definition of the domains and other graphical details as in Figure 2 of the Paper.

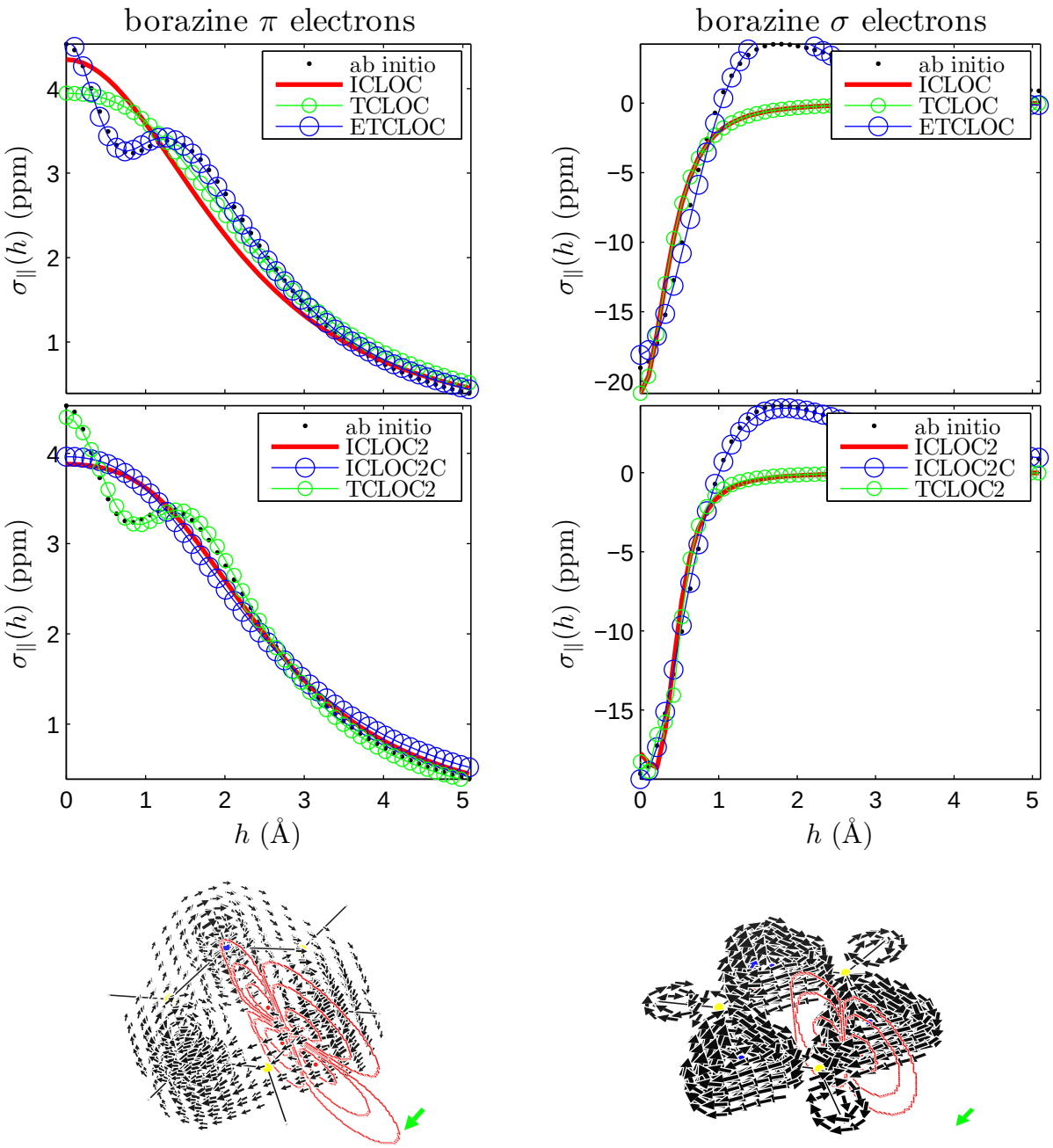

Figure 25: Scans of the contributions of π (top left) and σ (top right) electrons to the parallel component of magnetic shielding $\sigma_{\parallel} = -\mathrm{NICS}_{\parallel}$ computed *ab initio* and with different RCMs. On bottom the corresponding three-dimensional current density maps superposed on contour lines limiting domains D2, D16, D128 on the integration planes. The green arrow, corresponding to the maximum value of the π contribution to the current density in benzene (0.08 au) for a magnetic field perpendicular to the ring, is oriented in the diatropic sense. Definition of the domains and other graphical details as in Figure 2 of the Paper.

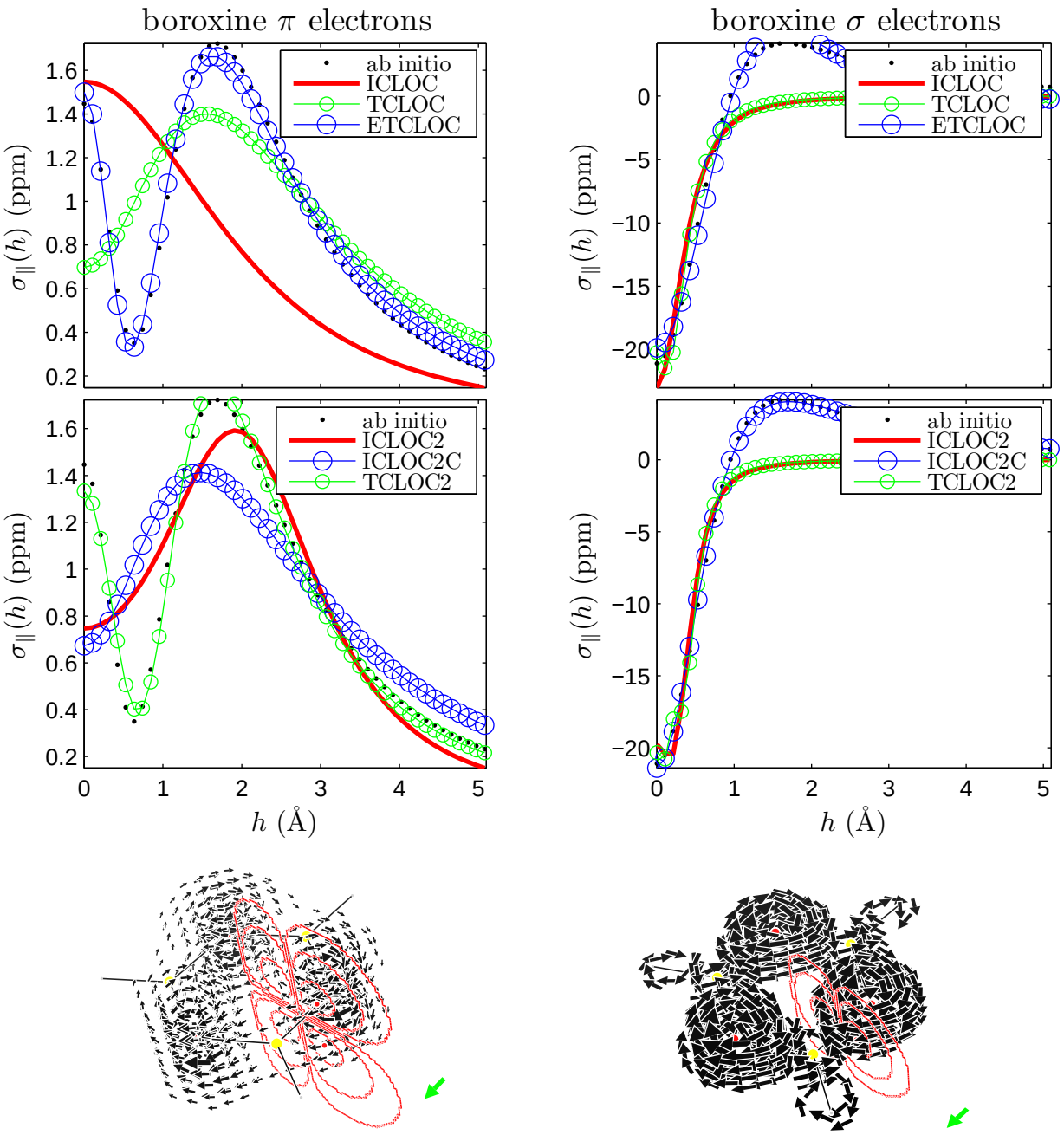

Figure 26: Scans of the contributions of π (top left) and σ (top right) electrons to the parallel component of magnetic shielding $\sigma_{\parallel} = -\mathrm{NICS}_{\parallel}$ computed *ab initio* and with different RCMs. On bottom the corresponding three-dimensional current density maps superposed on contour lines limiting domains D2, D16, D128 on the integration planes. The green arrow, corresponding to the maximum value of the π contribution to the current density in benzene (0.08 au) for a magnetic field perpendicular to the ring, is oriented in the diatropic sense. Definition of the domains and other graphical details as in Figure 2 of the Paper.

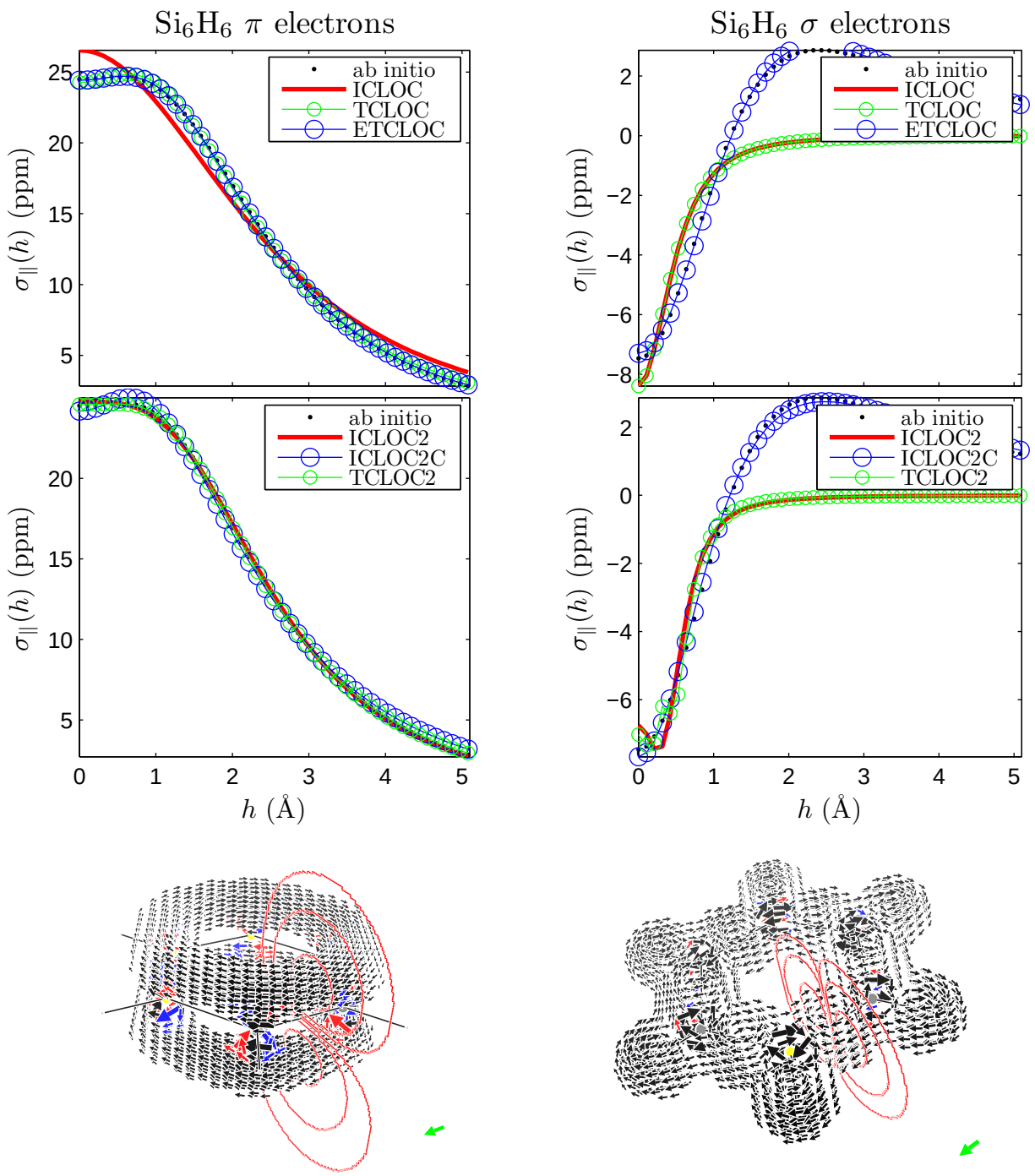

Figure 27: Scans of the contributions of π (top left) and σ (top right) electrons to the parallel component of magnetic shielding $\sigma_{\parallel} = -\mathrm{NICS}_{\parallel}$ computed *ab initio* and with different RCMs. On bottom the corresponding three-dimensional current density maps superposed on contour lines limiting domains D2, D16, D128 on the integration planes. The green arrow, corresponding to the maximum value of the π contribution to the current density in benzene (0.08 au) for a magnetic field perpendicular to the ring, is oriented in the diatropic sense. Definition of the domains and other graphical details as in Figure 2 of the Paper.

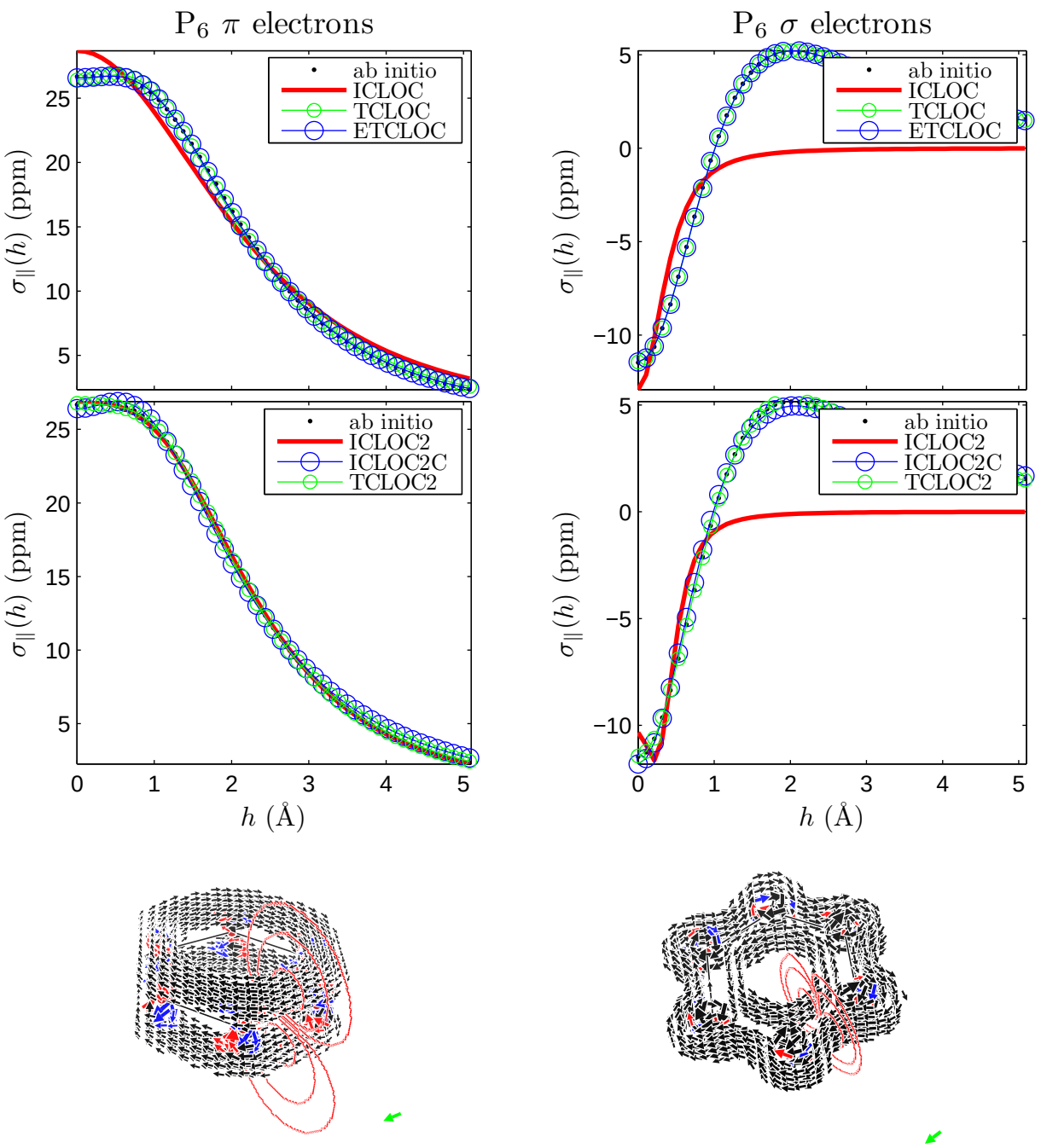

Figure 28: Scans of the contributions of π (top left) and σ (top right) electrons to the parallel component of magnetic shielding $\sigma_{\parallel} = -\mathrm{NICS}_{\parallel}$ computed *ab initio* and with different RCMs. On bottom the corresponding three-dimensional current density maps superposed on contour lines limiting domains D2, D16, D128 on the integration planes. The green arrow, corresponding to the maximum value of the π contribution to the current density in benzene (0.08 au) for a magnetic field perpendicular to the ring, is oriented in the diatropic sense. Definition of the domains and other graphical details as in Figure 2 of the Paper.

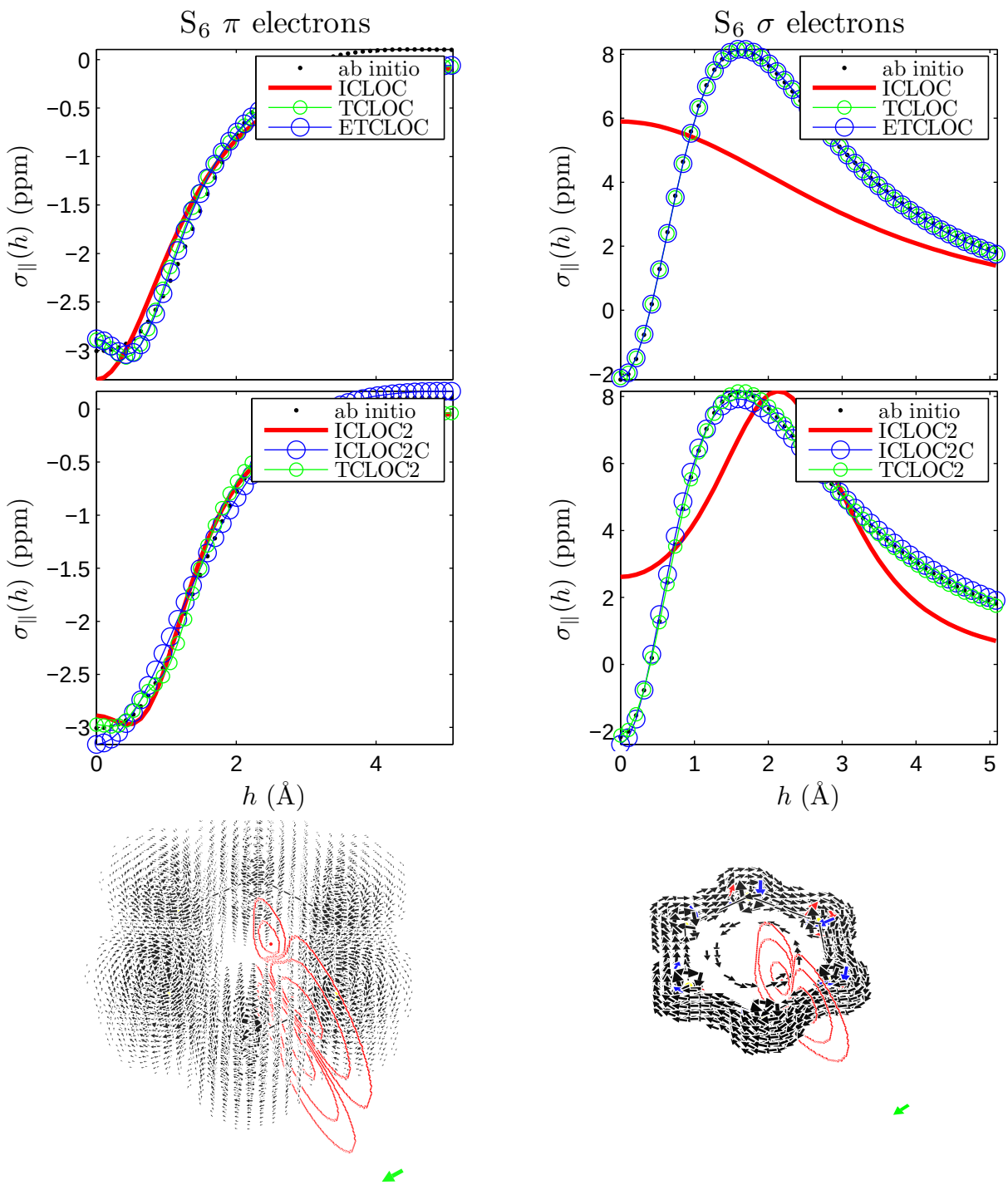

Figure 29: Scans of the contributions of π (top left) and σ (top right) electrons to the parallel component of magnetic shielding $\sigma_{\parallel} = -\mathrm{NICS}_{\parallel}$ computed *ab initio* and with different RCMs. On bottom the corresponding three-dimensional current density maps superposed on contour lines limiting domains D2, D16, D128 on the integration planes. The green arrow, corresponding to the maximum value of the π contribution to the current density in benzene (0.08 au) for a magnetic field perpendicular to the ring, is oriented in the diatropic sense. Definition of the domains and other graphical details as in Figure 2 of the Paper.

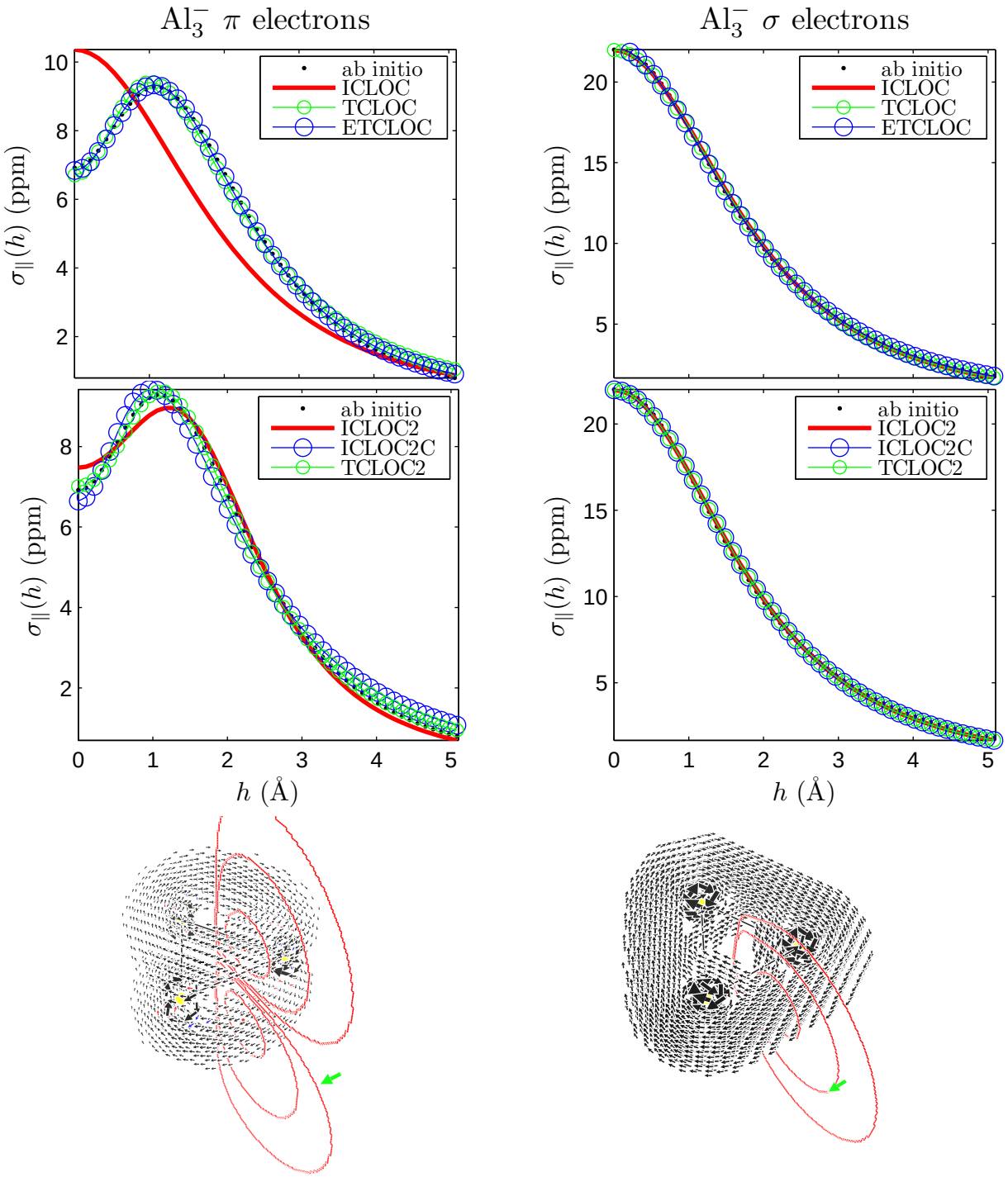

Figure 30: Scans of the contributions of π (top left) and σ (top right) electrons to the parallel component of magnetic shielding $\sigma_{\parallel} = -\mathrm{NICS}_{\parallel}$ computed *ab initio* and with different RCMs. On bottom the corresponding three-dimensional current density maps superposed on contour lines limiting domains D2, D16, D128 on the integration planes. The green arrow, corresponding to the maximum value of the π contribution to the current density in benzene (0.08 au) for a magnetic field perpendicular to the ring, is oriented in the diatropic sense. Definition of the domains and other graphical details as in Figure 2 of the Paper.

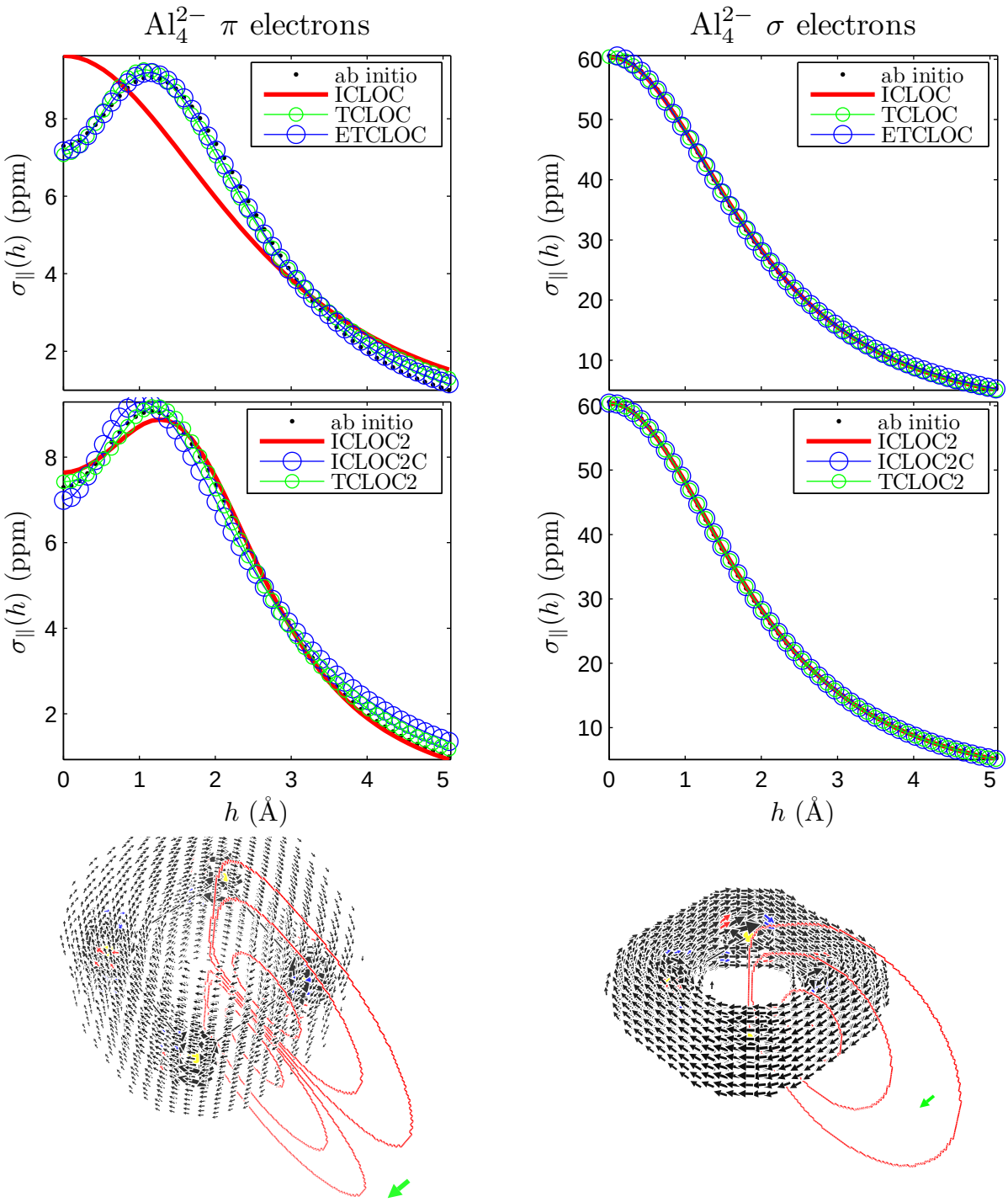

Figure 31: Scans of the contributions of π (top left) and σ (top right) electrons to the parallel component of magnetic shielding $\sigma_{\parallel} = -\mathrm{NICS}_{\parallel}$ computed *ab initio* and with different RCMs. On bottom the corresponding three-dimensional current density maps superposed on contour lines limiting domains D2, D16, D128 on the integration planes. The green arrow, corresponding to the maximum value of the π contribution to the current density in benzene (0.08 au) for a magnetic field perpendicular to the ring, is oriented in the diatropic sense. Definition of the domains and other graphical details as in Figure 2 of the Paper.

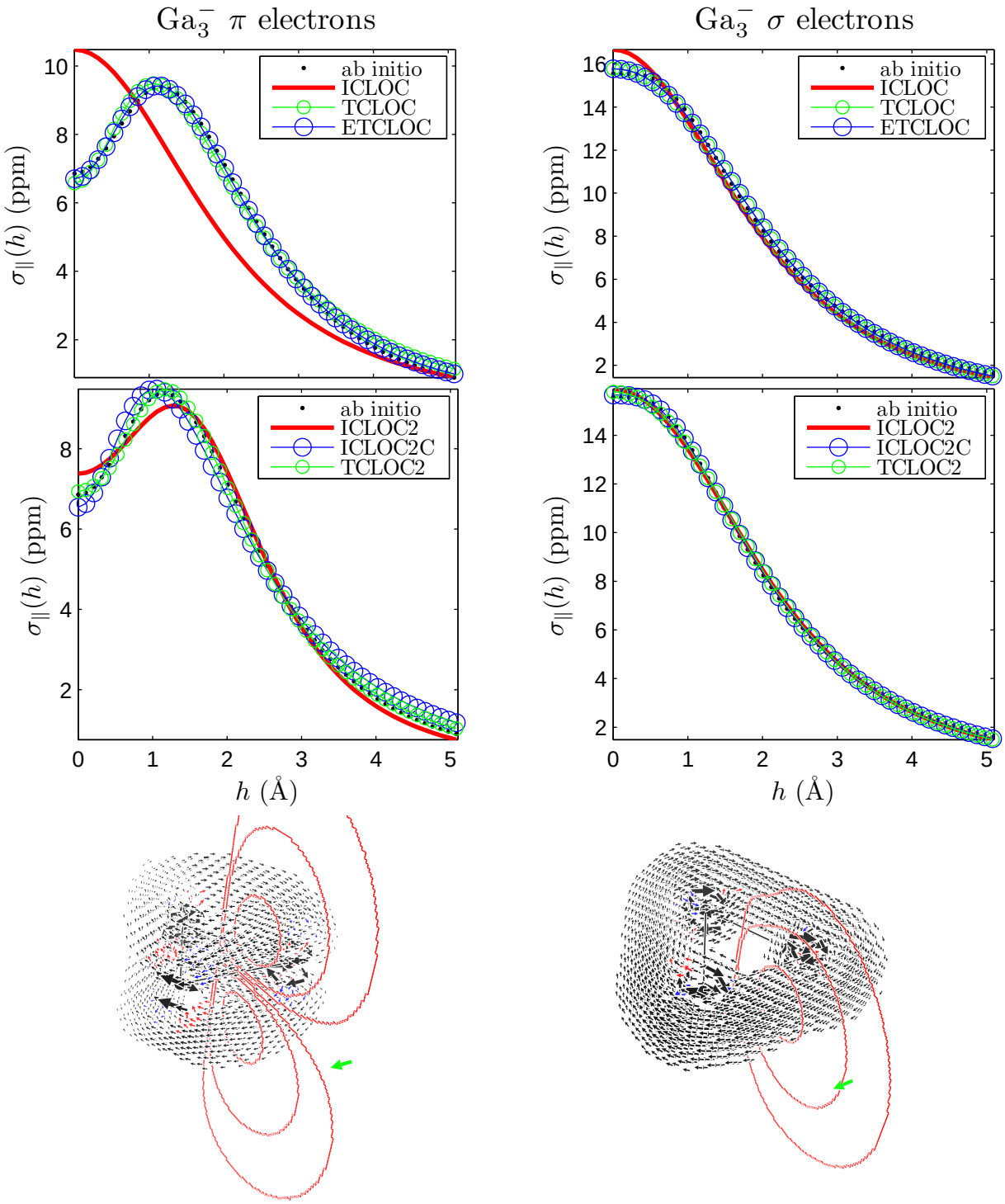

Figure 32: Scans of the contributions of π (top left) and σ (top right) electrons to the parallel component of magnetic shielding $\sigma_{\parallel} = -\mathrm{NICS}_{\parallel}$ computed *ab initio* and with different RCMs. On bottom the corresponding three-dimensional current density maps superposed on contour lines limiting domains D2, D16, D128 on the integration planes. The green arrow, corresponding to the maximum value of the π contribution to the current density in benzene (0.08 au) for a magnetic field perpendicular to the ring, is oriented in the diatropic sense. Definition of the domains and other graphical details as in Figure 2 of the Paper.

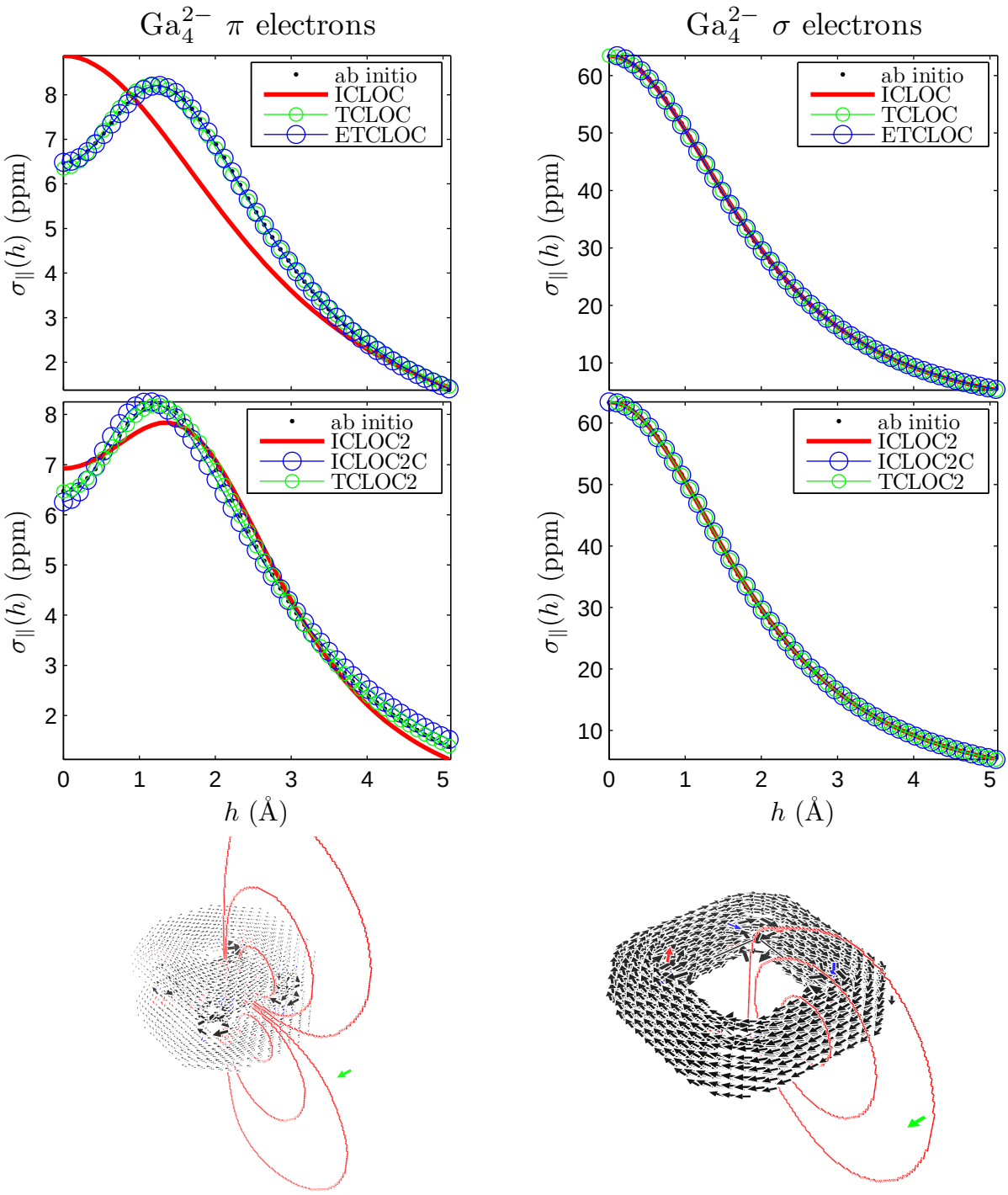

Figure 33: Scans of the contributions of π (top left) and σ (top right) electrons to the parallel component of magnetic shielding $\sigma_{\parallel} = -\mathrm{NICS}_{\parallel}$ computed *ab initio* and with different RCMs. On bottom the corresponding three-dimensional current density maps superposed on contour lines limiting domains D2, D16, D128 on the integration planes. The green arrow, corresponding to the maximum value of the π contribution to the current density in benzene (0.08 au) for a magnetic field perpendicular to the ring, is oriented in the diatropic sense. Definition of the domains and other graphical details as in Figure 2 of the Paper.